이학석사 학위논문

Characteristics of water-soluble organic aerosols in Seoul, Korea

서울 도심 용존유기에어로졸의 특성

2017 년 2 월

서울대학교 대학원

지구환경과학부

한 희 준

Characteristics of water-soluble organic aerosols in Seoul, Korea

서울 도심 용존유기에어로졸의 특성

지도교수 김 규 범
이 논문을 이학석사 학위논문으로 제출함

2017 년 12 월

서울대학교 대학원
지구환경과학부

한 희 준

한희준의 이학석사 학위논문을 인준함
2017 년 12 월

위 원 장 황 점 식 (인)
부위원장 김 규 범 (인)
위 원 남 성 현 (인)

Abstract

Characteristics of water-soluble organic aerosols in Seoul, Korea

Heejun Han

School of Earth and Environmental Sciences

The Graduate School

Seoul National University

Water-soluble organic matter (WSOM) in aerosols plays a significant role in atmospheric processes affecting on global climate system directly by absorbing and scattering solar radiation and indirectly by acting as cloud condensation nuclei (CCN) and as potential sources for further reactions. The light absorbing organic carbon in aerosol WSOM including brown carbon (BrC) and atmospheric humic-like substances (HULIS) also has a significant impact on climate forcing by absorbing the ultraviolet (UV) wavelengths and visible spectrum. However, despite the potential importance of aerosol WSOM to global biogeochemical cycle and climate system, current understanding of its chemical compositions, optical properties, and processes are still poorly understood. Therefore, the objective of this study is to identify the characteristics of aerosol WSOM using the concentrations of water-soluble organic carbon (WSOC), water-soluble organic nitrogen (WSON), inorganic ion species, stable carbon isotope ratios ($\delta^{13}C_{WSOC}$),

and fluorescence techniques at an urban metropolitan city, Seoul, Korea from March 2015 to January 2016.

A seasonal variation in the WSOC concentration ranged from 3.1 to 39.5 μg m^{-3} (mean: 16.1 μg m^{-3}) with higher values during cold seasons (Mar–May and Oct–Jan) and lower values during warm seasons (Jun–Sep). The water-soluble organic nitrogen (WSON) concentrations ranged from 0.8 to 81.7 μg m^{-3} (mean: 14.5 μg m^{-3}) with large variations over different seasons. The $\delta^{13}C_{WSOC}$ values ranging from –21.0 to –27.5‰ (mean: –24.0‰) had contrasting pattern in their seasonal variation compared to the WSOC concentration, which fall within the range of terrestrial C3 plants (–24.0 to –37.0‰) and anthropogenic fossil combustion sources (–25.0 to –32.0‰). In addition, a 10-day air mass back trajectory showed that most of air masses are transported from the East Asian continents except for summer indicating that continental outflow may become a powerful source influencing the organic carbon signature in Seoul.

The fluorescence property of aerosol WSOM and WSOC concentration exhibited a similar seasonal variation indicating the greatest similarity in their atmospheric process through a year. As the UV radiation intensity increases more than two folds during the summer (Jun–Sep), the fluorescence intensities of humic compounds in aerosol WSOM decreased approximately by 80% and the total WSOC concentration decreased approximately by 30% suggesting that humic fraction is more susceptible to UV irradiation. A linear relationship between the fluorescence intensity of humic components and UV radiation rate (r^2=0.4) indicates that atmospheric HULIS is predominantly controlled by photo-induced degradation. These results were also in good agreement with the experiment result.

The results suggest that aerosol WSOM in Seoul was mainly derived from terrestrial sources, and a significant change in fluorescence property of chromophores in aerosol WSOM was predominantly influenced by photo-induced degradation. The photochemical degradation plays a significant role in atmospheric optical property and might be an important sink for light absorbing organic compounds in ambient urban aerosols.

Keywords: organic aerosols, water-soluble organic matter, water-soluble organic carbon, HULIS, fluorescent dissolved organic matter, photochemical degradation

Student number: *2014-21312*

Table of Contents

List of Tables

List of Figures

1. Introduction

1.1 Atmospheric organic matter

Organic aerosols occur in two different forms as primary and secondary aerosols. Primary organic aerosols are directly emitted from the sources, while secondary organic aerosols are formed through chemical reactions in the atmosphere (Gelencser et al., 2007; Song et al., 2007). The primary organic aerosols can be categorized into natural and anthropogenic sources. Natural sources are derived from mineral dusts, soils, wildfires, volcanic eruptions, and marine organics, while anthropogenic sources are involving fossil fuel combustion, biomass burning, motor vehicle emissions, industrial, and agricultural particles. A known sink of atmospheric particles is wet and dry deposition (Mladenov et al., 2010). Wet deposition usually occurs through rain, snow, and fog describing the vertical scavenging of soluble gases and particles. Dry deposition refers to gases and aerosol particles suspending in the atmosphere, which can be subjected to long-range transport via air masses.

Organic aerosols play a significant role in atmospheric chemistry and global biogeochemical cycles on Earth. The major issues of organic aerosols contain various atmospheric processes, which can modify the global energy budget, air quality, and climate system (Duarte and Duarte, 2013; Ghan et al., 2007; Kirillova et al., 2014a). A hydrophilic nature of organic aerosols directly affect on climate forcing by absorbing and scattering solar radiation and indirectly by acting as cloud condensation nuclei (CCN) for cloud formation, which can be transported and deposited from the atmosphere to receptor regions (Kanakidou et al., 2005; Wozniak et al., 2012). Fine particulate aerosols also directly influence on climate

system and visibility combined with air pollutants (Zong et al., 2016). Moreover, it has been found to have a serious impact on human respiratory tract (Poschl, 2005).

A substantial fraction of atmospheric aerosols is known as water-soluble. In particular, atmospheric water-soluble organic carbon (WSOC) contributes 10–80% of total organic carbon content in aerosols (Duarte and Duarte, 2013; Kirillova et al., 2014b). The majority of WSOC is known to be composed of atmospheric humic-like substances (HULIS) approximately 15–60%, which are similar to terrestrial and marine-humic and fulvic acids characterized with colored or chromophoric components of dissolved organic matter (CDOM) (Graber and Rudich, 2006; Zappoli et al., 1999). Mostly known sources of atmospheric HULIS are terrestrial soil and plants, biomass burning, and marine organics (Graber and Rudich, 2006).

Recently, the light absorbing organic carbon compound has received growing attention due to its significant impact on climate forcing. Many studies found that WSOC contains light absorbing organic carbon called brown carbon (BrC) (including HULIS) in large portion (Andreae and Gelencser, 2006; Graber and Rudich, 2006; Kirillova et al., 2014a). Also, it has been found that BrC strongly absorbs in the ultraviolet (UV) wavelengths and visible spectrum, which is responsible for 7–19% of the global aerosol absorption (Chen et al., 2016; Hecobian et al., 2010). Although the light absorbing properties of BrC and HULIS are expected to be weaker than that of black carbon (BC), which absorbs a wide range of spectra from visible to near-infrared radiation, its contribution would be significant due to its higher abundance in the atmosphere (Hoffer et al., 2006).

Thus, understanding the absorbance and fluorescence property of light absorbing organic carbon is important in estimating the climate forcing and radiative budget in the atmosphere. However, despite the potential importance of water-soluble fraction of organic aerosols, current understanding of its chemical compositions, absorbance and fluorescence properties, and processes still remains uncertain and controversial.

1.2 Aim of this study

The overall goal of this study is to improve the current knowledge about the significance of atmospheric WSOM and its optical property (absorbance and fluorescence) in urban environment based on a yearlong monitoring of atmospheric organic aerosols in Seoul, Korea. The objectives of this study are:

[1] To identify the source of atmospheric WSOC in urban aerosols; and;

[2] To investigate the fluorescence property of aerosol WSOM and further to identify the major processes responsible for significant changes in fluorophores of WSOM in aerosols.

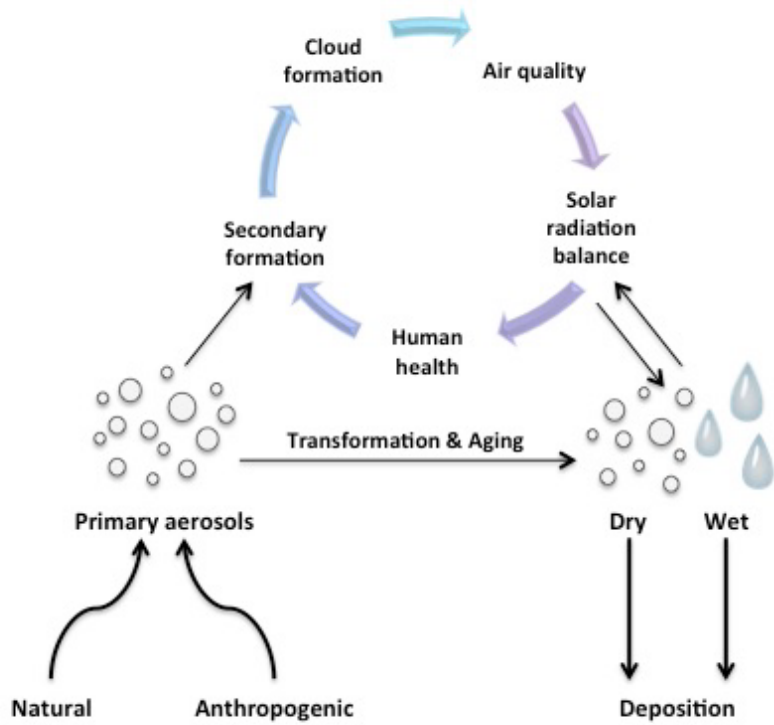

Figure 1. Atmospheric processes of organic aerosols.

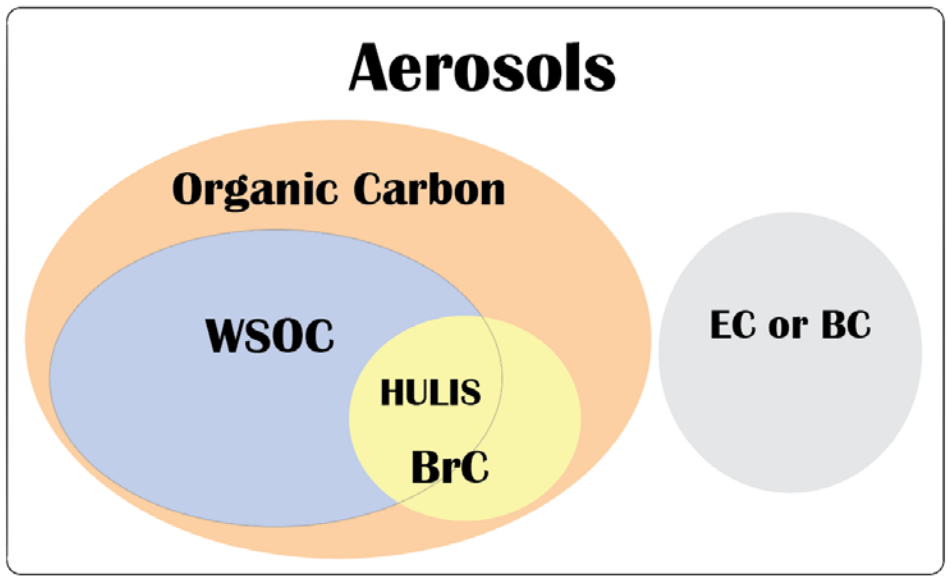

Figure 2. Schematic illustration of aerosols.

2. Materials and Methods

2.1 Study area and sample collection

Seoul is the capital of South Korea and one of the largest metropolitan cities in the world. The total geographical land area of Seoul is 605.25 km^2 with a population of over 10 million residents. Seoul is located in the northwest of the Korean peninsula, which is surrounded on all three sides by oceans: the East Sea, the South Sea of Korea, and the Yellow Sea. The study site is approximately 30 km away from the Yellow Sea (Figure 3).

South Korea has been highly affected by severe dust storms originated mostly from the Chinese and Mongolian deserts during the month of spring (Mar–May) and often in winter (Dec–Feb) (Lin et al., 2012). Asian dust, which is a seasonal or annual meteorological phenomenon in East Asia, travels all over China and drives across South Korea to Japan characterized with a period of high aerosol loading. Recently, the Asian fine dust-derived air pollution is mostly concerned and a focus of major environmental issue with highly increased anthropogenic emissions.

Aerosol samples (n=78) were collected using a high volume air sampler (HV-1000, SHIBATA, Japan) installed at the rooftop of the research institute in the Seoul National University in Seoul, Korea (37.5° N; 127° E, 20 m above ground level) from March 2015 to January 2016. Samples were collected for 24 hrs at a constant flow rate of 1000 L min^{-1} through the pre-combusted (450°C, 5 hrs) glass microfiber filters (GF/F, 8 inch × 10 inch, Whatman). The total air volume of samples was averaged to 1440 m^3, and *in situ* measurement of pressure and temperature were recorded. Blank samples were collected by exposing a blank

filter briefly at the study site and analyzed in the same way to other aerosol filter samples. Total suspended particulates (TSP) in aerosol filters were measured using mass differences of desiccated filters between pre- and post-sampling. Collected samples were covered with aluminum foil, placed in polyethylene bag, and store in the dark at −20°C until analysis.

Daily records of atmospheric particulate matters PM_{10} and $PM_{2.5}$, which are a mixture of fine solid particles with aerodynamic diameters less than or equal to 10 and 2.5 μm, and additional weather information of the study site including temperature, UV radiation rate, and precipitation rate were obtained from the ambient air quality monitoring network named AirKorea in Korea Environmental Corporation (KECO) and Korea Meteorological Administration (KMA).

In addition, the PM concentration of the study site (PM_S) was calculated using the mass of TSP and total air volume collected during sampling period to verify the regional representativeness of aerosol samples collected in the study site. The concentration of total PM_S was compared with the PM_{10} concentrations of other provinces in Korea provided from KECO and KMA (Figure 3). Significant positive correlations between PM_S and PM_{10} concentrations ($r^2>0.5$) were found in 8 different regions compare to the other fregions in Korea: Gyunggi ($r^2=0.61$; 20 km away from the study site), Incheon ($r^2=0.6$; 22 km), Chungbuk ($r^2=0.51$; 98 km), Chungnam ($r^2=0.57$; 84 km), Jeonnam ($r^2=0.53$; 310 km), Jeonbuk ($r^2=0.55$; 283 km), Daejeon ($r^2=0.55$; 142 km), and Gangwon ($r^2=0.53$; 150 km). The strongest correlation ($r^2=0.7$) was found with the PM_{10} concentration recorded at the Seoul monitoring station, which is the nearest station to the study site. The PM correlation data of aerosol sample collected in the study site was fully

representative of geographical region around the study site, which may covers approximately 70% of the total land area of South Korea including the entire land area along the west coast regions.

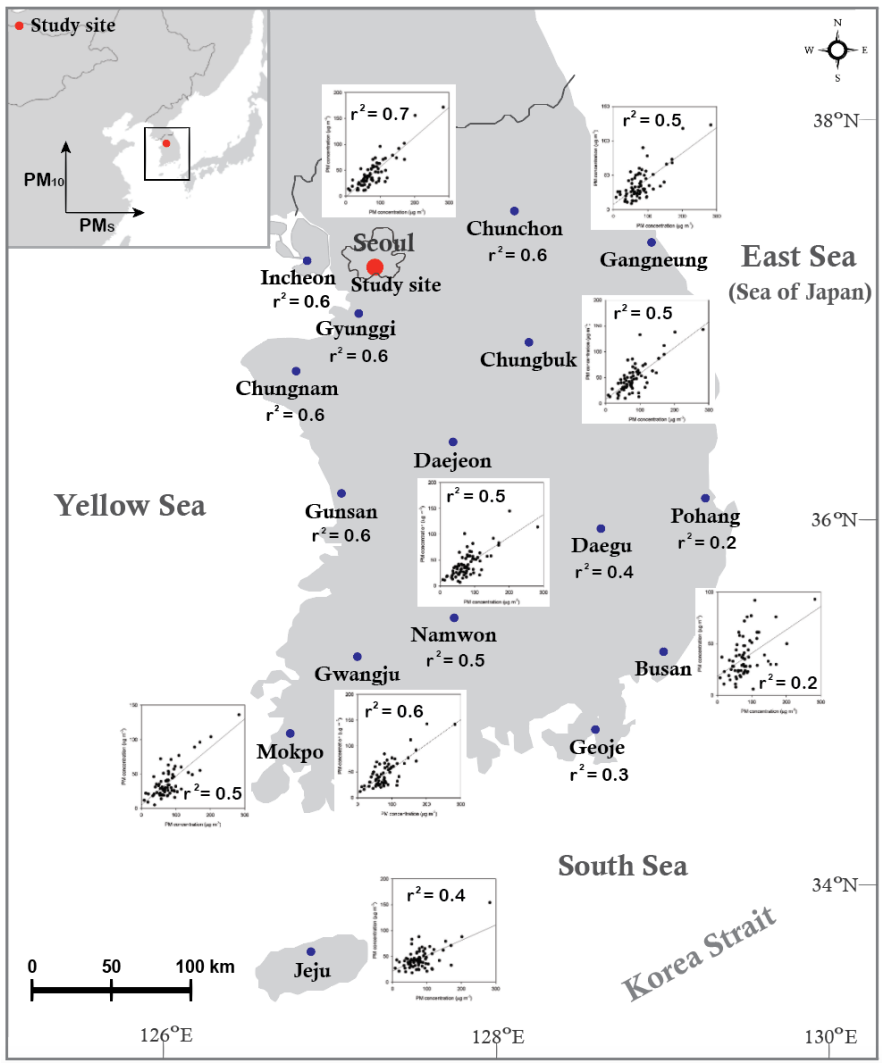

Figure 3. Map of geographical region around the study site with statistical relationships between PM_S (study site) (●) and PM_{10} concentrations of different regions in Korea during the sampling period.

2.2 Air mass back trajectory model

A 10-day air mass back trajectory was made using the National Oceanic and Atmospheric Administration (NOAA) Air Resources Laboratory's Hybrid Single-Particle Lagrangian Integrated Trajectory (HYSPLIT) model to reveal the source of aerosols and to understand general transport of air masses over the study region with a starting height of 20 m a. g. l. (Figure 4) (Stein et al., 2015). The model was computed using the meteorological data from the Global Data Assimilation System (GDAS) produced by NOAA (http://ready.arl.noaa.gov/HYSPLIT.php). The GDAS contains all available data from global satellite, aircraft reports, wind profile data, surface observations, and radar observations (Stein et al., 2015).

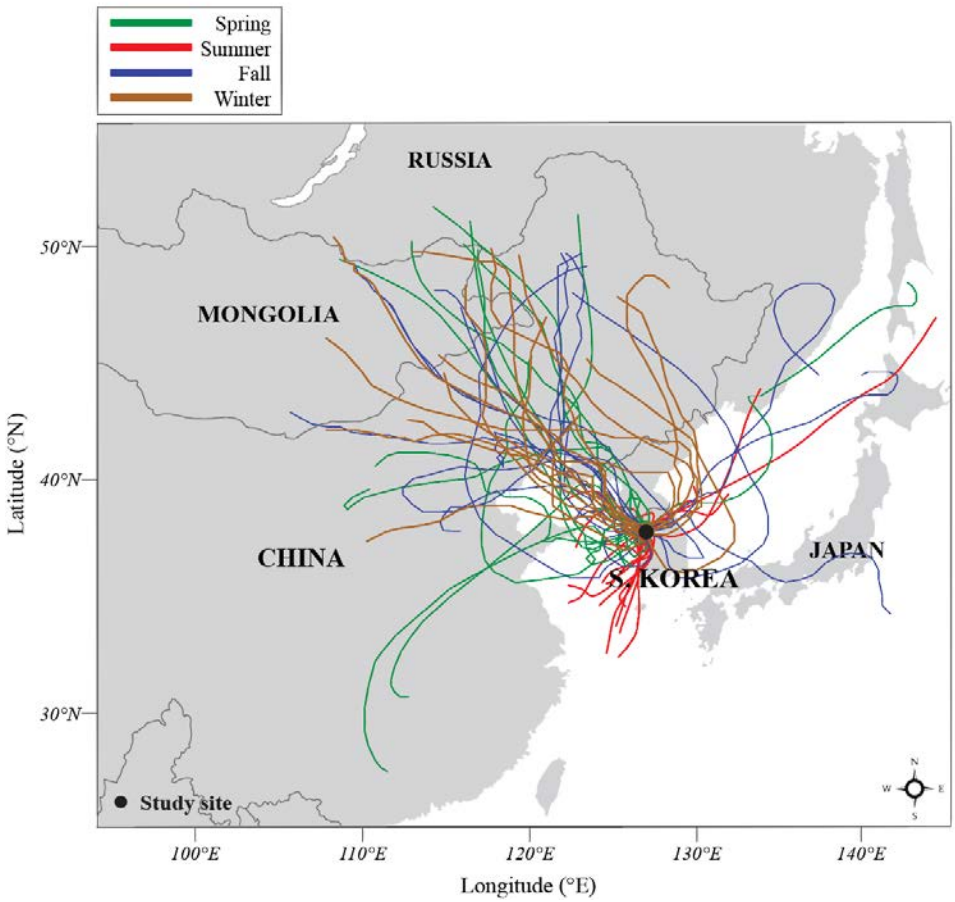

Figure 4. Map of geographical region around the study site (●) along with a 10-day air mass back trajectories of HYSPLIT model from March 2015 to January 2016.

2.3 Aerosol WSOM extraction and preparation

For the aerosol WSOM measurement, a small portion of filter paper (18 cm^2) was cut into small pieces (1 cm × 1 cm) and placed in a pre-HCl rinsed conical tube. The conical tube was subjected to extraction using 20 mL of deionized water and placed in the shaker table for 4 hrs at 125 rpm (Wozniak et al., 2012). The extracted solutions were filtered through a syringe filter (0.45 μm pore size Nucleopore, Whatman) and stored until analyses (Figure 5).

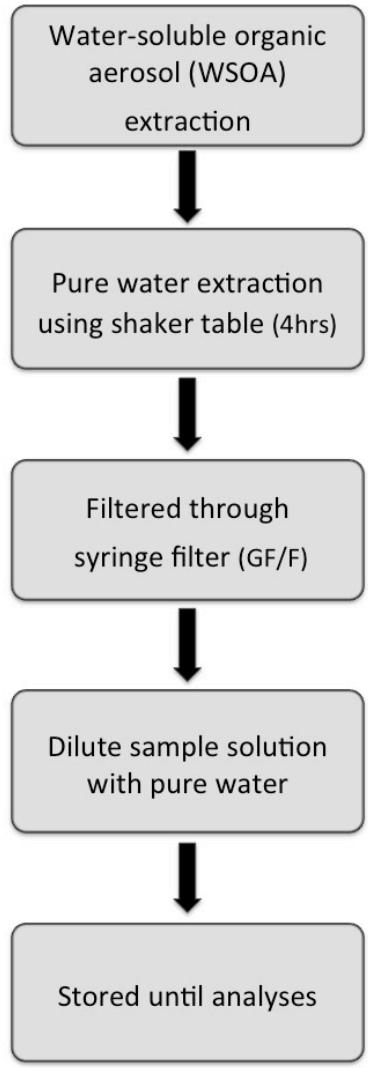

Figure 5. Methodological flow diagram for the aerosol WSOM extraction.

2.4 Analysis of WSOC and TDN

Duplicated samples for the WSOC and WSON analyses were acidified with 6M HCl in order to remove any inorganic carbon species exist in the solution. WSON concentration was calculated with the difference between total dissolved nitrogen (TDN) and inorganic nitrogen species, which are the sum of NO_2^-, NO_3^-, and NH_4^+. The concentrations of WSOC and TDN were measured by a high temperature oxidation method using a TOC-V analyzer (Shimadzu, Japan) (Figure 6). Acidified samples were sparged with carbon free air for 3 minutes to remove dissolved inorganic carbon and introduced into the combustion tube packed with platinum catalyst at 720°C. The concentrations of carbon dioxide and nitrogen monoxide were detected by a non-dispersive infrared detector (NDIR) and a chemiluminescence detector, respectively. The blank corrections were made using the WSOC measurement of blank filter. Standard solutions were performed using a potassium hydrogen phthalate ($C_8H_5O_4K$) (Peltzer et al., 1996). The accuracy and efficiency of instrument were qualified with the dissolved organic carbon (DOC) consensus reference material (CRM) of deep-sea reference water provided from Rosenstiel School of Marine and Atmospheric Science, University of Miami (http://yyy.rsmas.miami.edu/groups/biogeochem/CRM.html). The detection limit is 5.0 μmol L^{-1} for WSOC and 2.5 μmol L^{-1} for TDN.

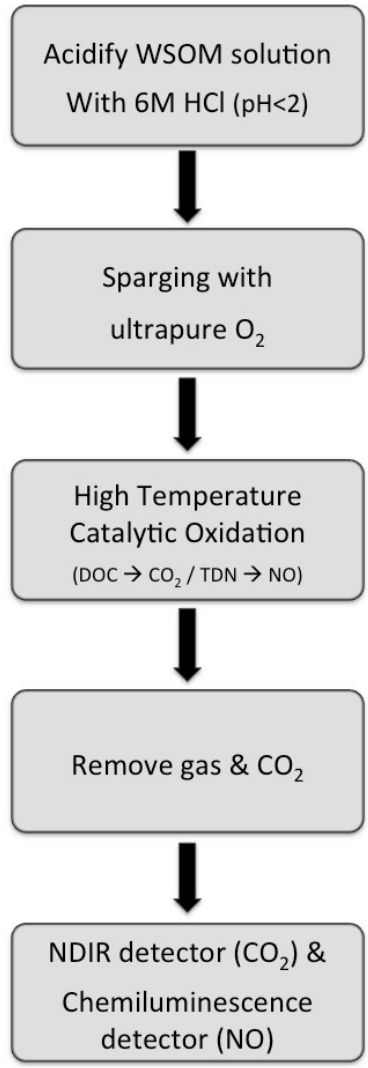

Figure 6. Methodological flow diagram for determination of WSOC and TDN with high temperature catalytic oxidation method using TOC analyzer.

2.5 Analysis of major ions

Major ion species were analyzed for determination of water-soluble anion (Cl^-, SO_4^{2-}, NO_3^-, and NO_2^-) and cation (Na^+, NH_4^+, K^+, and Ca^{2+}) species using high performance ion chromatography (HPLC, Waters 2695 system and 432 conductivity detector, USA) (Figure 7). Anions were analyzed using a borate/gluconate eluent with a flow rate of 2.0 mL min^{-1} and a Waters IC-Pak A HC column (4.6 mm × 150 mm) (Figure 8). Cations were analyzed using a 0.1 mmol L^{-1} ethylenediaminetetraacetic acid (EDTA) and 3.0 mmol L^{-1} HNO_3 as an eluent with a flow rate of 1.0 mL min^{-1} and a Waters IC-Pak C M/D column (3.9 mm × 150 mm) (Figure 9). The column temperature was maintained at 30°C and the samples were at 4°C during analysis.

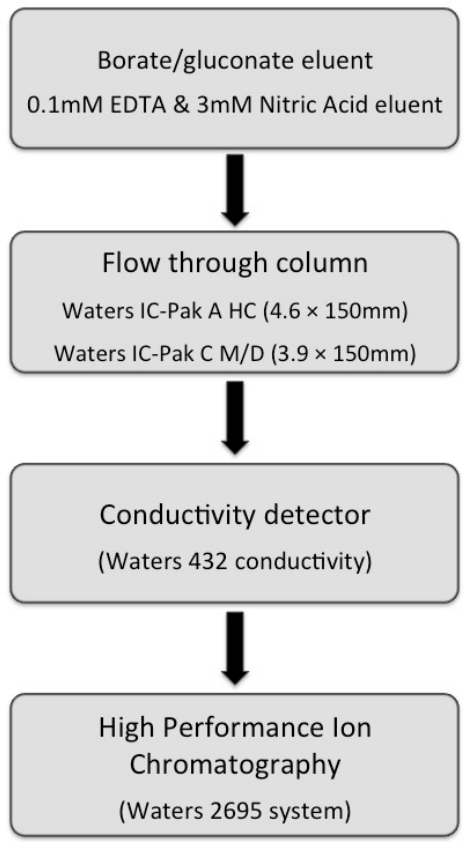

Figure 7. Methodological flow diagram for determination of major ion species using HPLC.

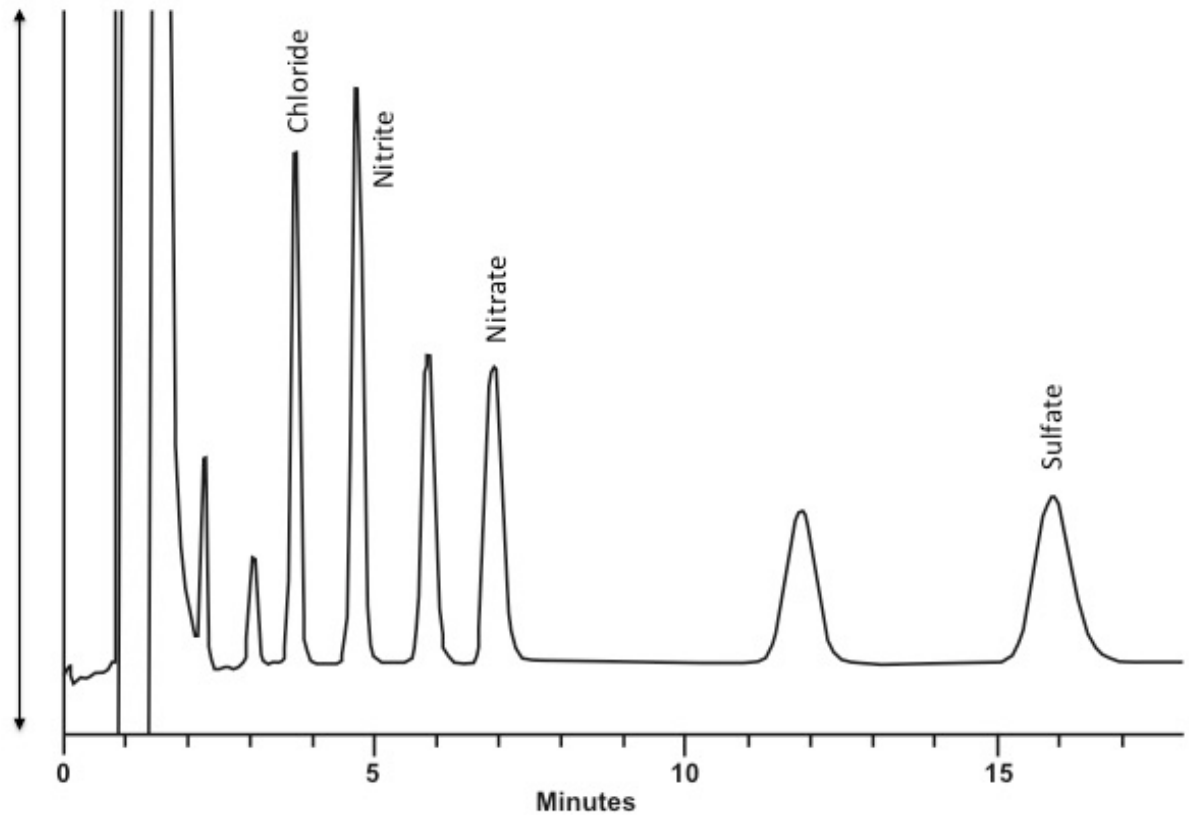

Figure 8. Alliance system for ion chromatography anion analysis.

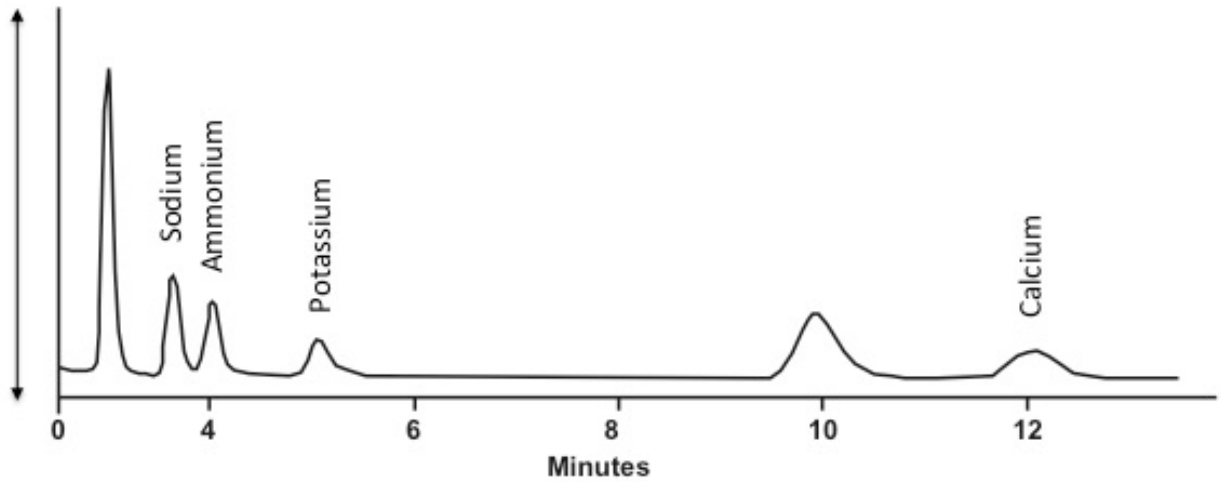

Figure 9. Alliance system for ion chromatography cation analysis.

2.6 Analysis of stable carbon isotope ratios

Stable carbon isotope ratio of WSOC ($\delta^{13}C_{WSOC}$) was measured using an isotope ratio mass spectrometer (Isoprime IRMS, Elementar, Germany) combined with TOC analyzer (vario TOC cube analyzer, Elementar, Germany) through an interface (vario Interface cube, Elementar, Germany) (Figure 10). Sample solutions were injected to TOC analyzer for high temperature combustion method to measure CO_2 using an NDIR detector and continuously flowed through a reduction column inside of an interface to IRMS. The isotopic composition $\delta^{13}C_{WSOC}$ were determined using the standard equation:

$$\delta^{13}C = \left(\frac{\left({}^{13}C / {}^{12}C\right)_{sample}}{\left({}^{13}C / {}^{12}C\right)_{standard}} - 1 \right) X\ 1000\ ‰$$

where Vienna Pee Dee Belemnite (PDB) was used as the isotope standard.

Analytical tests were conducted with sucrose (–10.45 ± 0.03‰, IAEA) and Suwannee River Fulvic Acid (SRFA) (–27.6 ± 0.12‰, IAEA) to evaluate recovery yields as well as the accuracy and precision of the measurements. The blank corrections were made using the CRM of low carbon water provided from Rosenstiel School of Marine and Atmospheric Science, University of Miami (http://yyy.rsmas.miami.edu/groups/biogeochem/CRM.html). Standard solutions for TOC analyzer were performed using a sucrose standard solution.

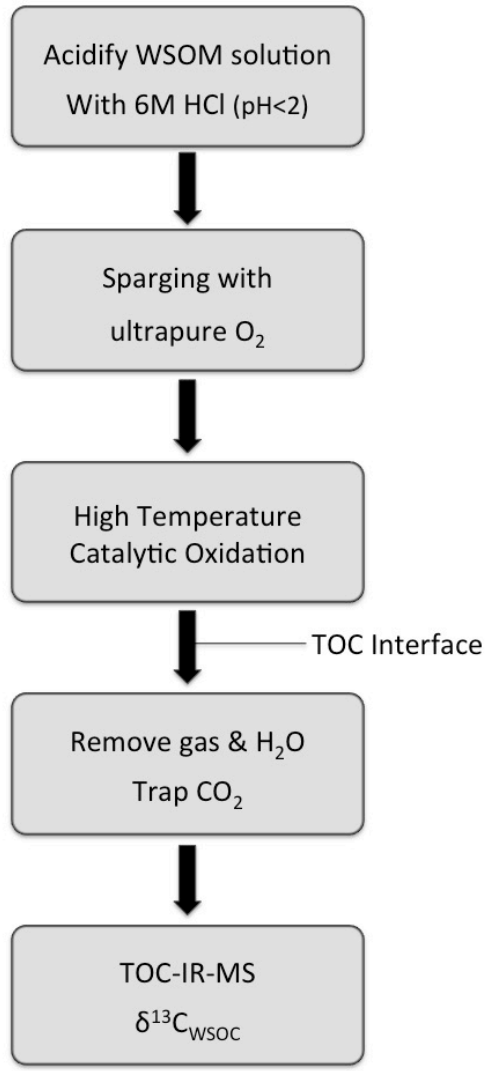

Figure 10. Methodological flow diagram for determination of stable carbon isotope ratios using TOC-IRMS.

2.7 Analysis of fluorescent WSOM and PARAFAC model

Excitation-emission matrix (EEM) spectroscopy is a common technique to determine the optical and structural properties of chromophores responsible for the light absorbance and fluorescence of organic matter. Previous studies had observed the optical properties, spectral characteristics, and potential sources of each component (Table 3). Five general types of fluorescence peaks have been identified in natural waters including terrestrial humic-like, marine humic-like, and protein-like fluorescence (Coble, 2007). In general, absorbance property and fluorescence property of organic matter are closely linked to each other and this significant relationship between two parameters may be used for modeling absorption spectra of chromophoric organic compounds including BrC and HULIS using fluorescence techniques (Green and Blough, 1994; Kieber et al., 2006; Mladenov et al., 2010; Santos et al., 2009).

Fluorescence spectroscopy of aerosol WSOM was performed by a spectrofluorometer (FS-2, SCINCO, Korea) using a 10 mm path length quartz cuvette (Figure 11). The emission and excitation wavelength ranges were set from 250 nm to 600 nm with 2 nm scanning intervals and from 250 nm to 500 nm with 5 nm scanning intervals, respectively. The fluorescence intensities were normalized using the values of a quinine sulfate dihydrate (QS) standard solution at the excitation/emission wavelength of 350/450 nm in quinine sulfate unit (QSU) (Velapondi and Mielenz, 1980). A QS standard solution was made using a quinine stock solution diluted in 0.1N sulfuric acid. Raman and Rayleigh scattering signals were removed.

The humification index (HIX) and fluorescence index (FI) were determined to evaluate microbial and terrestrial contributions to the WSOM (Table

4). The fluorescence indices, HIX (the ratio of integrated intensity of emission intensity in 435–480 nm at excitation intensity 255 nm to integrated intensity of emission intensity in 300–434 nm at excitation intensity 255 nm) and FI (the ratio of Ex/Em=370/470 nm to Ex/Em=370/520 nm), were calculated from EEM spectra (Birdwell and Engel, 2010; Fu et al., 2015). Fluorescence indices of EEM spectra were compared to estimate relative degree of maturation of organic matter and amount of organic matter derived from terrestrial and microbial sources (Birdwell and Engel, 2010; Fu et al., 2015).

Parallel factor analysis (PARAFAC) model was performed in the MATLAB R2013a program using the DOMFluor toolbox (Stedmon and Bro, 2008). PARAFAC model is a multi-way data processing method to find data-specific components (Bro, 1997). Prior to the modeling, Raman and Rayleigh scattering signals were excised (Zepp et al., 2004). The number of unique components was identified from the combined EEM data and the results were validated by split-half analysis and analysis using random initialization (Stedmon and Bro, 2008).

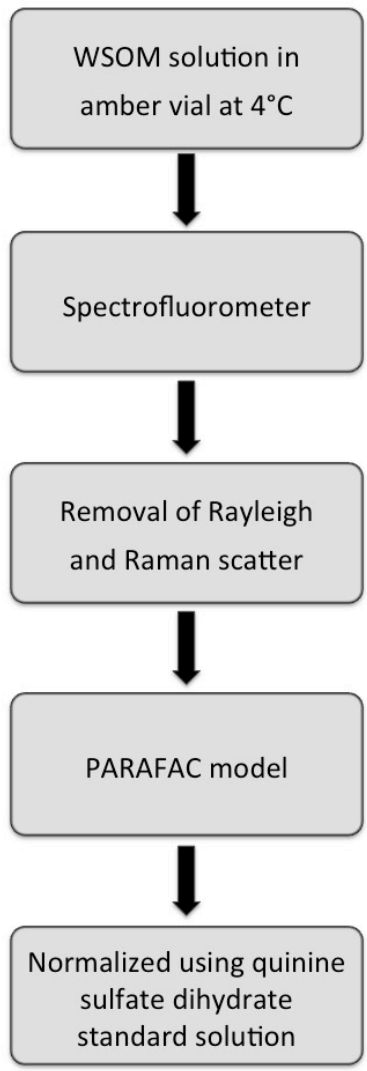

Figure 11. Methodological flow diagram for determination of fluorescence intensity of fluorescent WSOM in aerosols.

2.8 Photochemical degradation experiment

Laboratory experiment was conducted to evaluate the impact of solar UV radiation on fluorescence property of WSOM in aerosols using a small portion of aerosol filter sample inside of the incubator equipped with internal UV lamp (280–315 nm; UV-B). The incubator was maintained under positive air pressure with a constant temperature at 20°C.

Two comparative aerosol filter samples were selected randomly for each of the higher and lower fluorescent groups, which had a similar range of WSOC concentration. Summer aerosol sample (WSOC: 15.7 μmol L^{-1}) was collected in August 2015 and winter aerosol sample (WSOC: 18.7 μmol L^{-1}) was collected in December 2015. The UV radiation rate and the duration of sunshine was 18.5 MJ m^{-2} and 11.2hr for the summer aerosol sample and 5.4 MJ m^{-2} and 3.1hr, respectively, for the winter aerosol sample (KMA).

Each of non-irradiated aerosol samples was evaluated for the initial measurements. Samples were exposed for 1 day to 42 days (6 weeks) to simulated UV radiation. The photochemical degradation of chromophoric organic matter was evaluated by measuring the changes in the WSOM residue. Each sample was analyzed for the fluorescence intensities of WSOM and WSOC concentrations after the UV exposure.

3. Results

3.1 Air mass back trajectory

A 10-day air mass back trajectory model determined the source regions and transport pathways of air masses to the study site. Due to a regional meteorology of the study site, which is dominated by the East Asian Monsoonal effect, most air masses are transported from the arid and semi-arid regions in the Asian continent where the yellow dusts are blowing from especially during the spring (Mar–Apr) and often in winter (Nov–Jan). According to the trajectory model, almost all air masses in spring, fall, and winter were transported from the northeastern provinces of China, which accounted for approximately 64% of the total air masses to the study site (Figure 4). During the summer (Jul–Aug), all of the air masses were transported from the near surrounding oceans: the Yellow Sea, the South Sea, and the East sea. Approximately 85% of the air masses were transported from the Yellow Sea, while 13% of the air masses were transported from the East Sea.

3.2 Chemical compositions

A seasonal variation in the WSOC concentration was found ranging from 3.1 to 39.5 μg m^{-3} (mean: 16.1 μg m^{-3}) with relatively higher values during cold seasons (Mar–May and Oct–Jan) and lower values during warm seasons (Jun–Sep) (Figure 12A). The WSON concentration ranged from 0.8 to 81.7 μg m^{-3} (mean: 14.5 μg m^{-3}) (Figure 12A). Significantly higher values were found during spring (Mar–May) and fall (Oct–Nov) with a large seasonal variation. The concentrations of PM_{10} and $PM_{2.5}$ were typically higher during the Asian dust period (Mar–Apr) (Figure 12B). The stable carbon isotope ratios of WSOC ($\delta^{13}C_{WSOC}$) and WSOC concentration exhibited a distinct seasonal pattern through a year. The $\delta^{13}C_{WSOC}$ values ranged from –21.0 to –27.5‰ with an average value of –24.0‰ (Figure 12C). Highly enriched $\delta^{13}C_{WSOC}$ values were found during March, August, and October to November, while the most depleted values were found during June and October. The fluorescence intensity of chromophoric WSOM exhibited relatively similar seasonal variation with WSOC (Figure 12D). The UV radiation rate and temperature were gradually increased from March to August and decreased from August to January each season (Figure 12E). The precipitation was maximized during the summer (Jul–Sep) (Figure 12E). Specific inorganic species were used as a source indicator of various sources. The concentration of NH_4^+, which can be used as an indicator of agricultural livestock and fertilizer use, showed a large seasonal variation through a year with the higher values during the spring and harvest seasons (Oct–Dec) (Figure 12F). SO_4^{2-} and NO_3^- concentrations, which represents a source indicator of anthropogenic fossil fuel combustion, exhibited a similar seasonal variation (Figure 12G). Both concentrations were typically higher in March and May to September, and lower during April and October to December,

which showed quite different pattern from that of WSOC and WSON. K^+ and Ca^{2+}, which can be used as source indicators of biomass burning and terrestrial mineral dusts, showed relatively constant trend through a year suggesting that continuous inputs of terrestrial and biomass burning sources (Figure 12H). The contribution of marine organics was determined using the calculated sea-spray fraction in aerosol WSOM. The sea-spray fraction was calculated using Cl^- and Na^+ concentrations assuming that all Cl^- and Na^+ are originated from seawaters: sea-spray = Cl^- + 1.4468 Na^+ (Maenhaut et al., 2008). The estimated sea-spray contribution was relatively higher during July to September (Figure 12I). The fluorescence indices were used for the source identification of WSOC. The ratio of the protein-like fluorescence (protein-like peak T) to humic-like fluorescence (humic-like peak M) can be used as an indicator measuring relative contribution of protein-like marine derived organics (Fu et al., 2015). The ratio of fluorescence intensity of peak T to peak M showed the highest values in July to August and November and the lowest values in March and September (Figure 12J). The ratio was gradually increased from spring to summer.

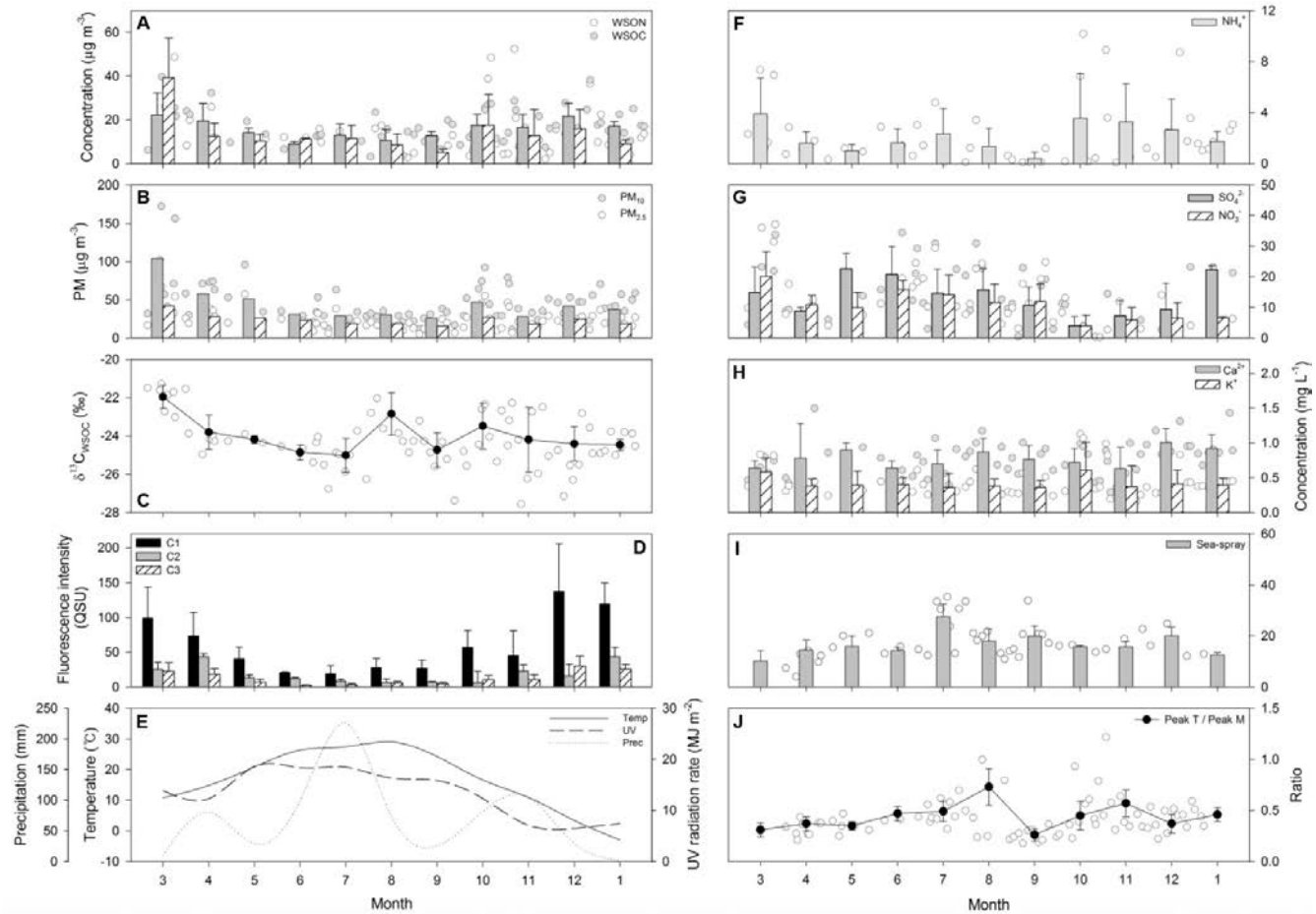

Figure 12. Temporal variations of the concentration of (A) WSOC and WSON, (B) PM_{10} and $PM_{2.5}$, (C) $\delta^{13}C_{WSOC}$, (D) fluorescence intensity of fluorescent components, (E) UV radiation rate, precipitation, and temperature, (F) concentrations of NH_4^+, (G) SO_4^{2-} and NO_3^-, (H) Ca^{2+} and K^+, (I) sea-spray concentration, and (J) the ratio of fluorescence intensities of peak T to peak M from 2015 to 2016 in Seoul.

Table 1. Ambient meteorological conditions, concentrations of major components, stable carbon isotope ratios, and fluorescence spectral parameters for the aerosol WSOM in Seoul.

Components	Temperature [°C]	UV radiation [MJ m^{-2}]	Precipitation [mm]	WSOC [μg m^{-3}]	WSON [μg m^{-3}]	PM_{10} [μg m^{-3}]	$PM_{2.5}$ [μg m^{-3}]	$\delta^{13}C_{WSOC}$ [‰]	Peak T / Peak M
Min	*–8.7*	*3.1*	*0.0*	*3.1*	*0.8*	*7.3*	*5.3*	*–27.5*	*0.18*
Max	*31.9*	*25.8*	*80.0*	*39.5*	*81.7*	*190.2*	*67.2*	*–21.0*	*1.22*
Mean	*15.5*	*14.5*	*9.4*	*16.1*	*14.5*	*42.9*	*23.3*	*–24.0*	*0.42*
Median	*15.8*	*14.6*	*4.5*	*15.7*	*9.6*	*37.4*	*21.4*	*–24.3*	*0.38*

Table 2. Concentrations of major ion species in the aerosol WSOM in Seoul.

Components	**NH_4^+ [mg L^{-1}]**	**SO_4^{2-} [mg L^{-1}]**	**NO_3^- [mg L^{-1}]**	**K^+ [mg L^{-1}]**	**Ca^{2+} [mg L^{-1}]**	**Na^+ [mg L^{-1}]**
Min	*0.1*	*4.0*	*0.3*	*0.2*	*0.3*	*1.9*
Max	*10.2*	*35.3*	*37.1*	*1.1*	*1.5*	*13.9*
Mean	*2.2*	*17.9*	*11.3*	*0.4*	*0.8*	*8.9*
Median	*1.2*	*9.4*	*9.8*	*0.4*	*0.8*	*8.8*

3.3 Fluorescence property

The spectral characteristics were evaluated to identify the fluorescence property of WSOM in ambient urban aerosols. Three major fluorescent components (C1 to C3) were identified using the PARAFAC model (Figure 13). Component 1 (C1) represented a strong peak at excitation/emission wavelength of 305/416 nm. The spectral characteristics of C1 refer to those of the peak M, and it was also assigned to humic-like component. Component 2 (C2) showed a single peak at 290/340 nm, which is similar to those of tryptophan- and protein-like peak T. Component 3 (C3) had two excitation maxima at 365 and 275 nm, and one emission maxima at 484 nm. The spectral characteristics of C3 were similar to the peak C, and it was also assigned to humic-like component.

In this study, the fluorescence indices ranged from 0.3 to 4.4 for the HIX and from 1.6 to 3.3 for the FI (Table 4). High HIX values correspond to strongly humified terrestrial sources, while low values (<4) are from autochthonous or microbial origin (Birdwell and Engel, 2010; Huguet et al., 2009). FI values of 1.4 or less correspond to terrestrial-derived organics with high aromacity, while low values of 1.9 or higher are microbial sources (Birdwell and Engel, 2010; Fu et al., 2015). Compared plots between the fluorescence indices are often used to determine the sources and humification stage of the WSOM in urban aerosols.

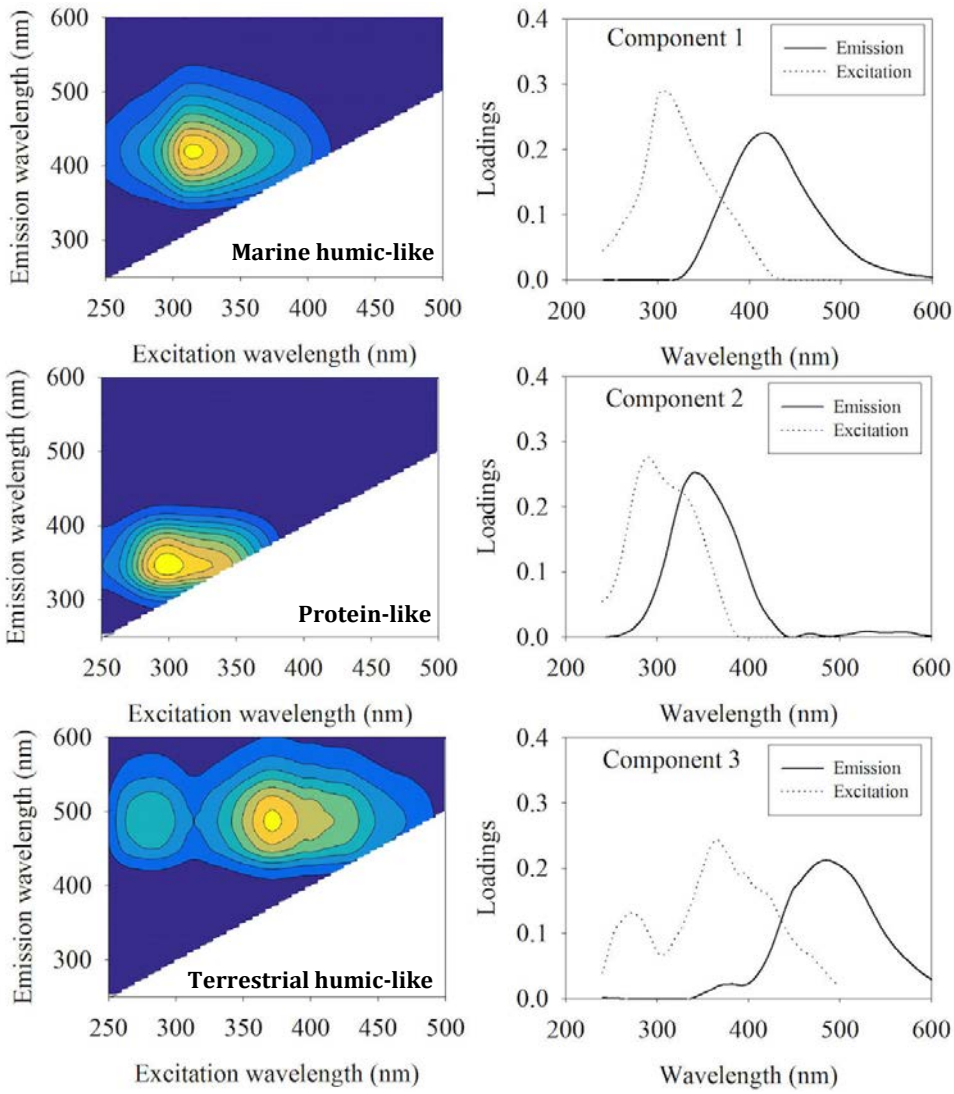

Figure 13. Contour plots of three components (C1 to C3) and excitation-emission loadings identified by the PARAFAC model for the aerosol WSOM samples in Seoul.

Table 3. Spectral characteristics of the FDOM components identified by the PARAFAC model for the aerosol WSOM samples.

Component	Ex/Em wavelengths [nm]	Peak	Description and origin	References
C1	305/416	M	Marine humic-like component derived from biological and microbial activities	C3: 250 (310)/400 nm (Kowalczuk et al., 2009) C6: 250 (320)/400 nm (Stedmon and Markager, 2005) C6: 325 (260)/385 nm (Yamashita et al., 2008)
C2	290/340	T	Protein-like (tryptophan-like) component derived from autochthonous processes	C7: 280/344 nm (Stedmon and Markager, 2005) C5: 280 (240)/368 nm (Stedmon et al., 2003) C6: 250 (290)/356 nm (Kowalczuk et al., 2009) C4: 280/318 nm (Yamashita et al., 2008)
C3	365/484	C	Terrestrial humic-like component derived from the terrestrial sources and autochthonous processes	C2: 250 (385)/504 nm (Stedmon and Markager, 2005) C4: 250 (360)/440 nm (Stedmon and Markager, 2005) C3: 370/496 nm (Murphy et al., 2006) C1: 260 (370)/466 nm (Yamashita et al., 2010) C4: 270 (390)/508 nm (Kowalczuk et al., 2009) C2: 345/433 nm (Yamashita et al., 2008)

Table 4. The fluorescence indices of the aerosol WSOM in Seoul.

Parameters	Min	Max	Mean	Median
HIX	*0.3*	4.4	1.7	1.7
FI	*1.6*	3.3	2.1	2.0

3.4 Photochemical degradation experiment

After 6-week UV exposure, two aerosol filter samples showed contrasting results in their residuals. For the winter aerosol sample, the final measurements of the WSOC concentration and fluorescence intensity of humic component were reduced by 25% and 52%, respectively, from the initial value (Figure 14A). In contrast to the winter sample, no significant changes were observed in both the WSOC pool and fluorescence property with the summer aerosol sample during the 6-week treatment (Figure 14B). The fluorescence intensity of protein-like component did not show any significant change during the 6-week treatment for both samples.

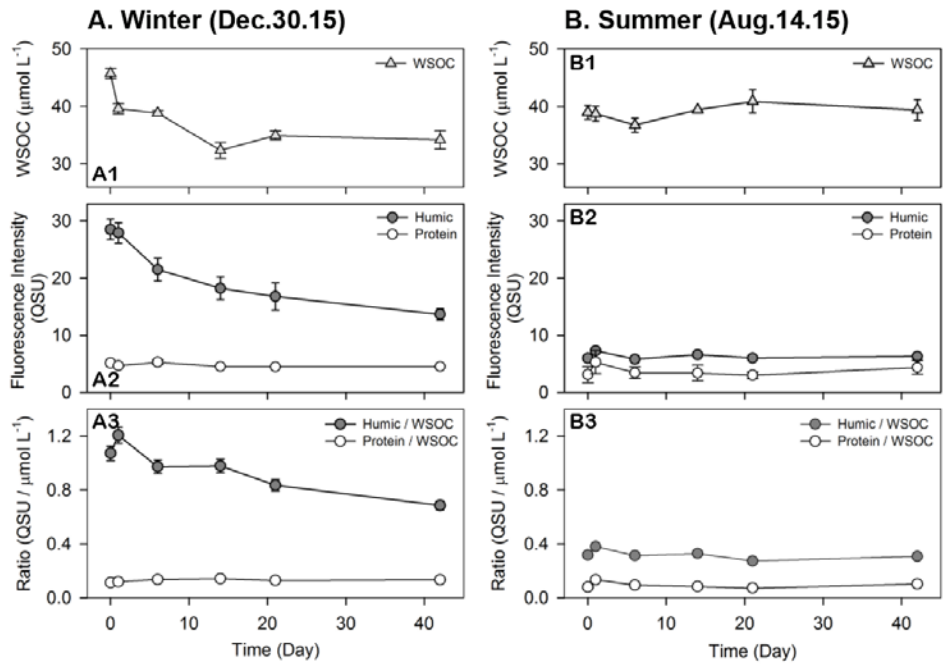

Figure 14. The WSOC concentrations of (A1) the winter and (B1) the summer aerosol samples, the fluorescence intensity of humic- and protein-like components of (A2) the winter and (B2) the summer aerosol samples, and the ratios of fluorescence component to WSOC of (A3) the winter and (B3) the summer aerosol samples with increasing UV irradiation time during the photochemical degradation experiment.

4. Discussion

4.1 Chemical property

The concentrations of WSOC and inorganic ion species were evaluated in order to identify the source of WSOC in Seoul. A good correlation (r^2=0.6) was found between the concentrations of WSOC and WSON (Figure 15A). The linear correlation analysis suggested that ratio of C/N of organic aerosols indicating the presence of different proportion of different nitrogen species. The closer or further spatial regression explains that relative contribution of different compositions of airborne organic matters (Kieber et al., 2005; Yan and Kim, 2015). The correlations between the concentrations of WSOC and other inorganic species had no significant relationship indicating that no single major source was defined in this study site (Figure 15B–E). The concentrations of NH_4^+ showed a positive correlation (r^2=0.4) with the WSOC concentration. NH_4^+ is usually derived from a gaseous NH_3, which is commonly found during agricultural activities (Meng et al., 2014). The concentration of NH_4^+ was higher during fall (Sep–Nov) indicating increased contribution of agricultural signature in this season. In general, K^+ is found in plants and crustal dust, which can be used as marker for biomass burning (Bosch et al., 2014). Ca^{2+} is derived from both crustal and marine sources (Gabriel et al., 2002). The concentrations of K^+ and Ca^{2+} showed no significant change through a year (Figure 15C). However, K^+ exhibited relatively good correlation (r^2=0.3) with the WSOC concentration compared to other marker species suggesting that WSOC can be highly associated with biomass burning of terrestrial C3 plant source. Both K^+ and Ca^{2+} were slightly higher during the spring (Mar–May) and fall (Sep–Nov) seasons due to higher contributions of continental-

derived aerosols. Air mass back trajectory model also suggested enhanced contribution of continental-derived aerosols during these seasons (Figure 4). Relatively constant level of K^+ and Ca^{2+} regardless of air mass transport pattern suggests that source might be originated in regional or local scale. The correlations between the WSOC concentration and concentrations of SO_4^{2-} and NO_3^- showed diffusely scattered patterns indicating no significant relationship (Figure 15D). Both SO_4^{2-} and NO_3^- are emitted from fossil fuel combustion, where NO_3^- is mainly derived from NO_2^- emitted from fossil fuel combustion (Bosch et al., 2014; Dentener et al., 2006). Also, no significant relationship was observed between the concentrations of WSOC and sea-spray, which means no significant contribution of marine organics (Figure 15E).

The temporal variations of $\delta^{13}C_{WSOC}$ values were quite different to the WSOC concentration. The $\delta^{13}C$ is a powerful tool in source defining due to a unique signature of different carbon fractions (Miyazaki et al., 2012). Previous studies have observed the isotopic compositions of various potential sources of organic carbon in aerosols (Figure 16). In Seoul, the $\delta^{13}C_{WSOC}$ values ranged from –21.0 to –27.5‰ (mean: –24.0‰), which fall within the range of terrestrial C3 plants (–24.0 to –37.0‰) and anthropogenic fossil and oil combustion sources (–25.0 to –32.0‰) (Figure 16) (Cachier, 1989; Fu et al., 2015; Kelly et al., 2005). The median values of $\delta^{13}C_{WSOC}$ were almost maintained between –24.0 and –26.0‰ suggesting that WSOC can be highly associated with the anthropogenic fossil fuel combustion and terrestrial sources. It has been widely known that there are higher influence of biomass burning of terrestrial C3 plants and anthropogenic fossil sources on WSOC in urban regions (Kirillova et al., 2014b). Also, previous study has reported that atmospheric dissolved organic carbon (DOC) in the

precipitation over Seoul is highly associated with the fossil fuel combustion (Yan and Kim, 2012). Although the level of organic contents and chemical compositions in precipitation and aerosols are not exactly coincident due to its contrasting origins of air masses and chemical reactions in atmosphere, many studies have suggested that anthropogenic emissions has made the largest contribution on the urban atmospheric WSOC (Duarte and Duarte, 2013; Kundu and Kawamura, 2014; Singh et al., 2016). In addition, approximately 67% of coal power plants are located along the west coast regions and near the study site (Appendix). According to the Korean government reports, more than half amount of fine particulate matter in Korea is originating from local source emissions including motor vehicles, factories, and coal power plants (Greenpeace, 2015). This suggests that local biomass burning of terrestrial C3 plants and anthropogenic fossil combustion sources can possibly influence on WSOC as one of the major contributors in Seoul.

There were significant changes in the $\delta^{13}C_{WSOC}$ values compared to the yearlong average value (–24.0‰) that highly enriched $\delta^{13}C_{WSOC}$ values were found distinctively during March, August, and October to December (Figure 12C). According to the previous studies, there are several processes influencing the isotopic composition such as removal by wet deposition, dilution effect, mixing of the emissions from other sources, and photochemical aging during the atmospheric oxidation processes (Aggarwal and Kundu, 2008; Bosch et al., 2014; Kirillova et al., 2014b; Miyazaki et al., 2012).

In March, highly enriched $\delta^{13}C_{WSOC}$ values (n=8; mean: –21.9‰) were coincident with higher concentrations of continental-derived PM_{10} and $PM_{2.5}$ during the Asian dust period (Figure 17). The potential source of highly enriched $\delta^{13}C_{WSOC}$ values can be derived from C4 vegetation, CAM plant, and carbonates

source emissions originated from the deserts or arid regions in China and Mongolia. The $\delta^{13}C$ values of C4 vegetation (corn, sugarcane, grasses), CAM plants (pineapple, aloe, cactus), and carbonates ranged from –6.0 to –19.0‰, –11.0 to –27.0‰, and +1.0 to –11.0‰, respectively (Figure 16) (Kelly et al., 2005; Smith et al., 1971). In China, deserts and C4 grassland cover approximately 40% of the total land area that may be a potential source region (Wang and Ma, 2016). A corn, which is a C4 crop, planting field covers approximately 21% of the total agricultural area in China (Hu and Zimmer, 2013). Recently, it has been observed that $\delta^{13}C$ values of aerosol total carbon (TC) ranged from –27.6 to –19.5‰ due to a combined contribution of C3 and C4 plants combustion in the Sanjiang Plain in northeast China (Cao et al., 2016). Also, previous study compared the $\delta^{13}C$ values of airborne carbonates between dust storm and non-dust-storm periods at a continental site Xi'an in China (Cao et al., 2005). The $\delta^{13}C$ value of airborne carbonates changed from –8.3‰ to –2.7‰ during the dust storm period indicating significant influence of mineral dust emissions from the near desert areas (Cao et al., 2005). The $\delta^{13}C$ value of soil carbonate increased as the amount of carbonate content increases during the dust storm events (Wang et al., 2005). Consequently, airborne carbonate originated from soil dust could be an important potential source of water-soluble fraction of organic aerosols. Thus, these results suggest that continental-derived dust aerosols might lead to highly enriched $\delta^{13}C_{WSOC}$ values in March.

In October and December, $\delta^{13}C_{WSOC}$ values showed significantly large variations ranging from –22.3 to –27.6‰ and almost all air masses (96%) were transported from the northeastern provinces of China, while the remainder were transported over the East Sea (Figure 4). During this season, a sudden increase in

the concentrations of WSON, NH_4^+, and PM_{10} was observed (Figure 12). A larger variance in $\delta^{13}C_{WSOC}$ values would reflects a greater mixing of various source emissions in this period. During September to December, continental outflow of open-field burning and domestic burning of crop residue are the possible sources influencing WSOC in Seoul. Relatively high concentrations of K^+ and NH_4^+, which are the indicators of biomass burning and agricultural livestock or fertilizer uses, suggest an enhanced contribution from the agricultural straw burning during and after the harvest seasons (Sep–Dec). Recent study has observed that the impact of agricultural biomass burning outflow from China to the air quality of the East Asian region was estimated to be over 56% (Huang et al., 2013). Thus, enhanced continental-derived agricultural biomass burning sources might contribute a large variance of $\delta^{13}C_{WSOC}$ values during September and December.

Many studies have suggested that photochemical aging by photochemical breakdown of longer-chain carbon compounds can be resulted in ^{13}C enrichment (Aggarwal et al., 2008). In August, $\delta^{13}C_{WSOC}$ values (n=5) ranged from –21.0 to –22.8‰ when the air masses were mainly originated from near surrounding oceans: the Yellow Sea, the South Sea, and the East Sea. During the summer, almost all air masses were transported from the surrounding oceans and about 85% of air masses were derived from the Yellow Sea (Appendix). In this period, clean air masses travelled from the source region to the receptor region without any other source intervention and directly exposed to the higher rate of solar UV radiation during their transport. Studies have shown that aerosol photochemical aging processes induce a fractionation in the aerosol $\delta^{13}C$, which leads to more positive $\delta^{13}C$ values in the aerosols (Aggarwal et al., 2008; Kirillova et al., 2014a). At the same time, the fluorescence ratios, a source indicator measuring relative contribution of

protein-like organics, were greatly enhanced up to 1.3 from July to August. In general, the fluorescence ratios were maintained almost constant near 0.5 through a year, except for summer (Jul–Aug) and October.

The fluorescence indices, HIX and FI, were compared to evaluate the relative contribution of different sources of organic matter in urban aerosols (Birdwell and Engel, 2010; Fu et al., 2015). In this study, the fluorescence indices of aerosol WSOM fall within the range of both terrestrial- and microbial-derived organics, but more weighted towards the microbial origin organics (Figure 18). During the summer (Jul–Aug), the fluorescence indices corresponded to a predominantly microbial origin, which can be derived from marine organics emitted from the ocean surface layer. More humified characters were found from the aerosol samples collected during the spring season (Mar–Apr), which tended to have more terrestrially humified characteristics.

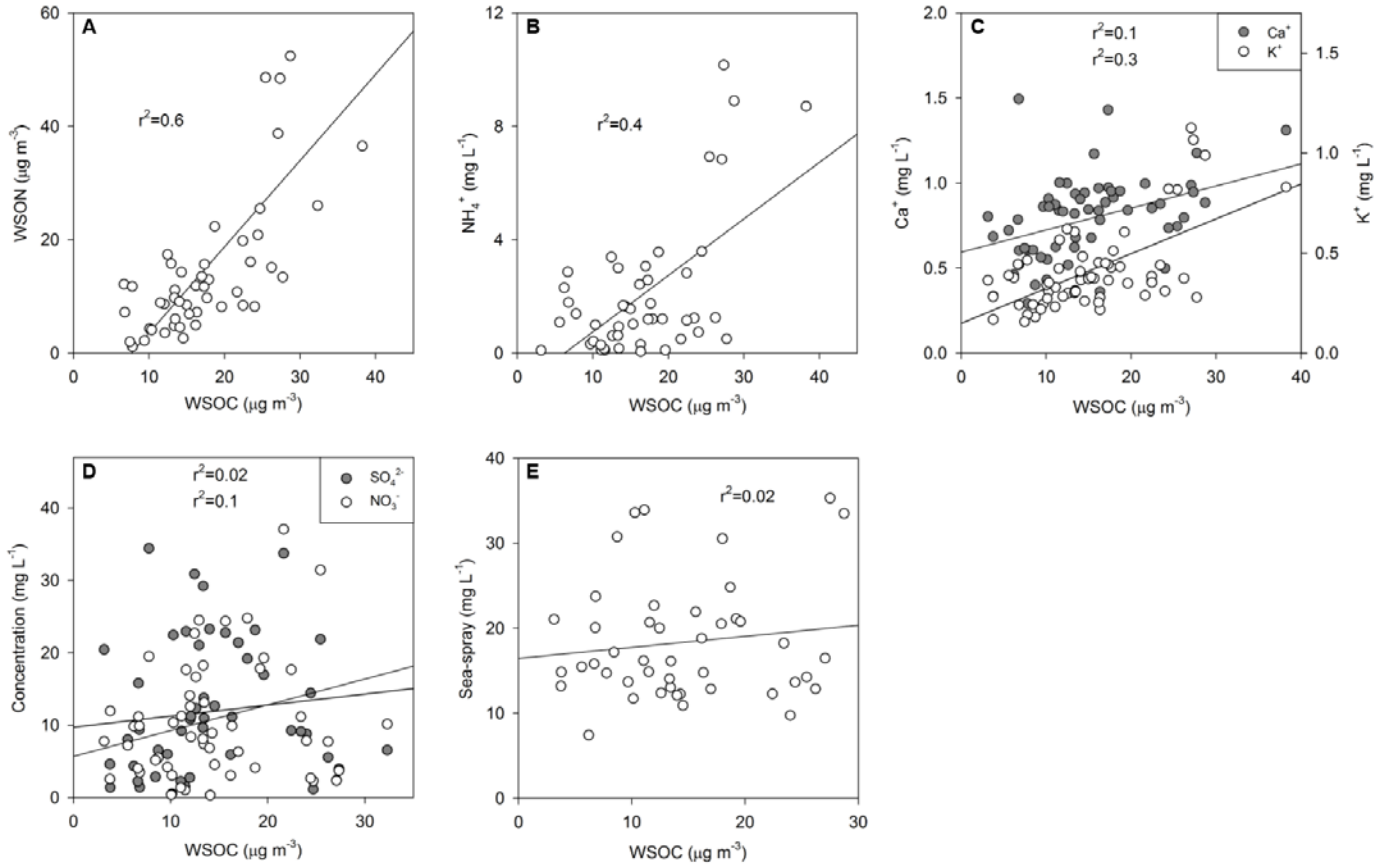

Figure 15. Linear correlations between the concentrations of (A) WSOC and WSON, (B) WSOC and NH_4^+, (C) WSOC and Ca^{2+} and K^+, (D) WSOC and NO_3^- and SO_4^{2-}, and (E) WSOC and sea-spray in Seoul, Korea.

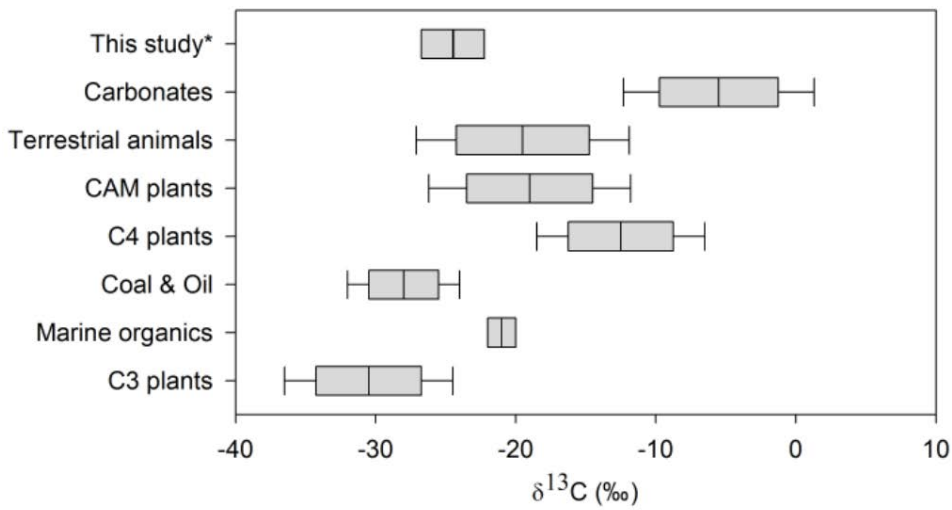

Figure 16. $\delta^{13}C$ measurements of potential sources of organic carbon in aerosols.

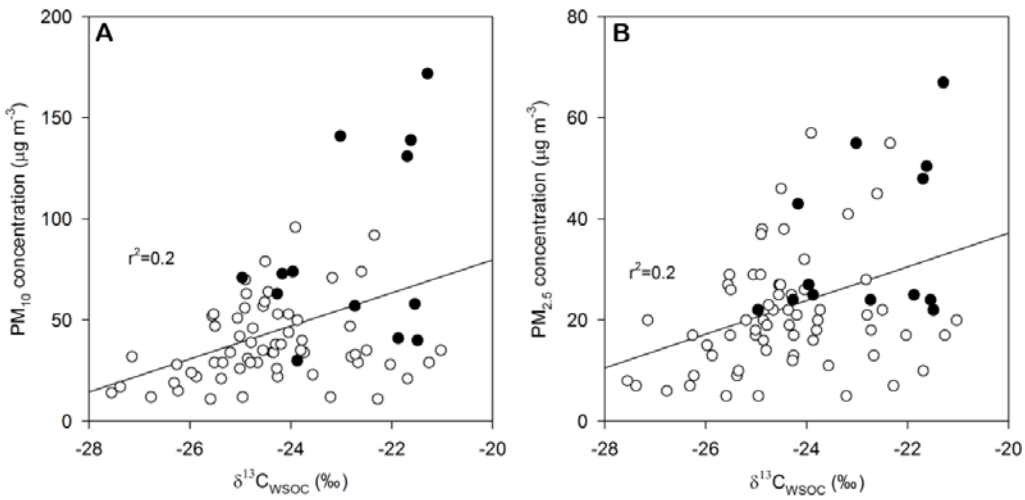

Figure 17. Linear correlations between the (A) $\delta^{13}C_{WSOC}$ and concentrations of PM_{10} and (B) $PM_{2.5}$. Filled circles are for samples collected during the Asian dust period (Mar–Apr).

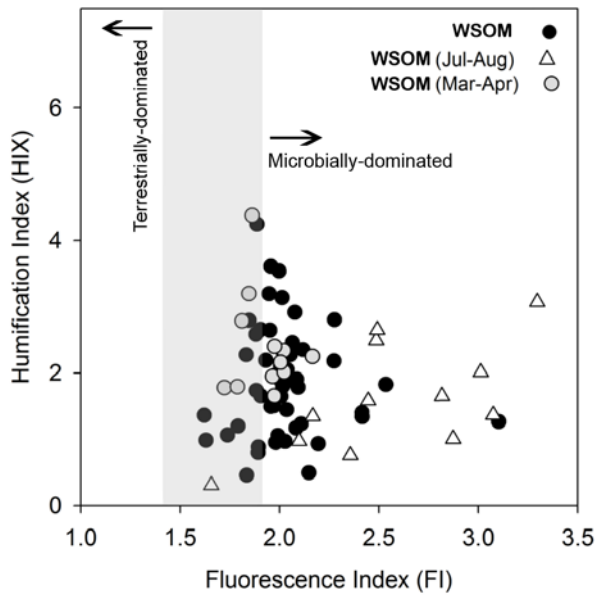

Figure 18. Comparison plots of the fluorescence index (FI) and the humification index (HIX) for the aerosol WSOM samples in Seoul.

4.2 Fluorescence property

The fluorescence intensity of chromophric aerosol WSOM exhibited a large seasonal variation, which showed a similar variation with the WSOC concentration. The fluorescence intensity of each component was normalized by the WSOC concentration to adjust different datasets for quantitative analysis of WSOM and compared with the UV radiation rate (Figure 19). The WSOC concentration showed a good correlation (r^2=0.6) with the fluorescence intensity of humic-like components (C1 and C3), which are responsible for a HULIS fraction of organic aerosols (Figure 20A). This indicates that HULIS and WSOC are highly associated with their amounts and distributions in urban environment. The correlation (r^2=0.3) between the WSOC and the protein-like component (C2) was less effective than the humic components (Figure 20B).

The statistically negative correlations were observed between the fluorescence intensities of each component (C1, C2, and C3) and UV radiation rate (Figure 21). The relationship was more effective for the HULIS fraction (C1) than the protein-like fraction (C2). The seasonal-averaged fluorescence intensity of HULIS and WSOC concentration were gradually decreased approximately by 80% and 30% from cold season (Oct–Dec) to warm season (Jun–Sep), respectively, as the UV radiation rate increases more than two folds (Figure 22). This indicates that the intensity of solar UV radiation greatly contributed to the degree of photo-induced degradation. Thus, the results suggest that HULIS fraction of organic aerosols is predominantly degraded by solar UV irradiation.

These results were also in agreement with the laboratory experiment conducted under stimulated UV radiation. Photochemical degradation targets the chromophoric components that absorbs and fluoresces at certain wavelengths of

light, which may change the chemical composition and spectral shape of light absorbing organic matter in the atmosphere (Mladenov et al., 2009). The humic selective photochemical degradation of aerosol WSOM was resulted in greater reduction in fluorescence intensity and total organic carbon content in WSOM pool for the winter aerosol sample, indicating loss of chromophores in aerosol WSOM as a result of photodegradation (Figure 14A and 23A). However, no significant fluorescence changes occurred in summer aerosol sample during the 6-week UV exposure (Figure 14B and 23B). Prior to the experiment, the spectral shapes of each aerosol sample were different from starting material that humic-like peak M is the one dominant component with a noticeable spectral feature in winter sample, while the summer sample has invisible peaks near the spectrum wavelength range of humic-like and protein-like components in equivalent magnitudes. This reflects that the summer aerosol sample appeared to consist largely of photo-refractory WSOC pool, while the winter aerosol sample was largely photo-labile WSOC. Photo-refractory residue in summer aerosol sample might be already photodegraded on exposure to natural solar radiation in the atmosphere. These results suggest that humic-like fluorescence materials in aerosol WSOM are more susceptible to photo-induced degradation.

In contrast, the fluorescence intensity of protein-like component did not show any significant change during the 6-week treatment for both samples, indicating that protein-like (tryptophan-like) chromophores in aerosol WSOM could be insusceptible to photo-induced degradation. Previous studies have found that protein-like or amino acid-like chromophores from autochthonous microbial activity is known to be more resistant to photobleaching and photochemical degradation in aquatic environment due to its different sources, structural

arrangement bounded with tryptophan or tyrosine, optical properties, and diagenesis (Birdwell and Engel, 2010; Helms et al., 2013; Zhang et al., 2013). This may explain the constant spectral feature in protein-like component maintaining during the 6-week UV exposure.

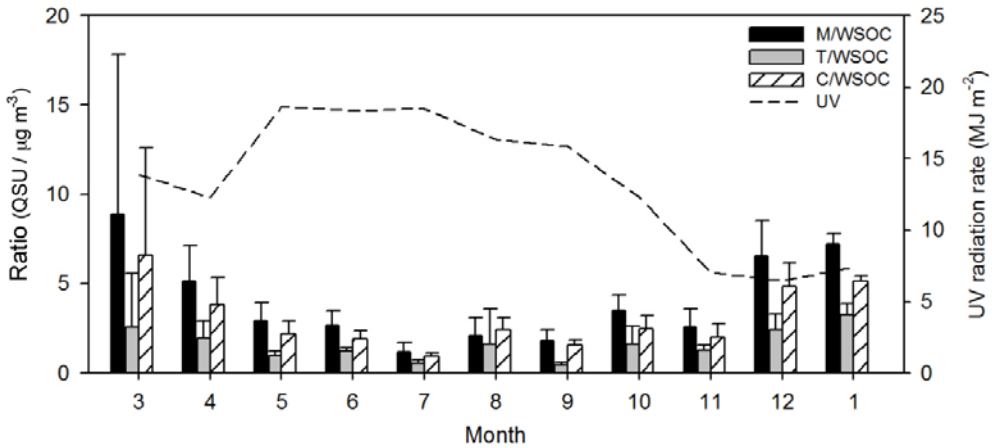

Figure 19. Temporal variations of the UV radiation rate and the monthly-averaged ratios of fluorescence intensities of components (humic-like: peak M and C; protein-like: peak T) to the WSOC concentrations in aerosol WSOM from March 2015 to January 2016 in Seoul.

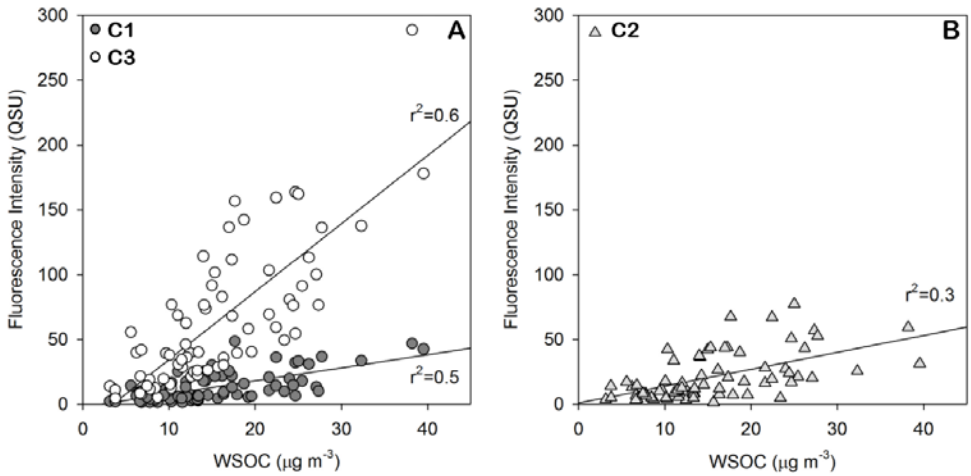

Figure 20. Linear correlations between the WSOC concentration and (A) the fluorescence intensities of humic-like components (C1 and C3), and of (B) the fluorescence intensities of protein-like component (C2) from March 2015 to January 2016 in Seoul.

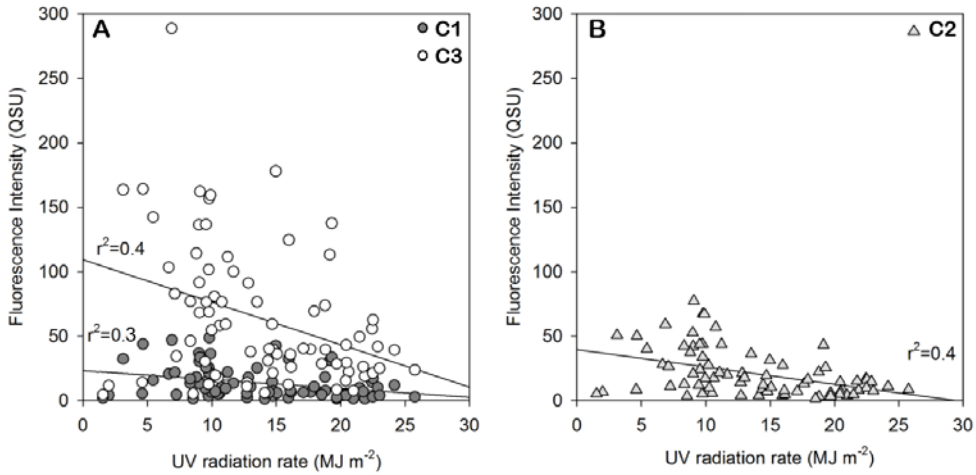

Figure 21. Linear correlations between the UV radiation rate and (A) the fluorescence intensities of humic-like components (C1 and C3), and of (B) the protein-like component (C2) from March 2015 to January 2016 in Seoul.

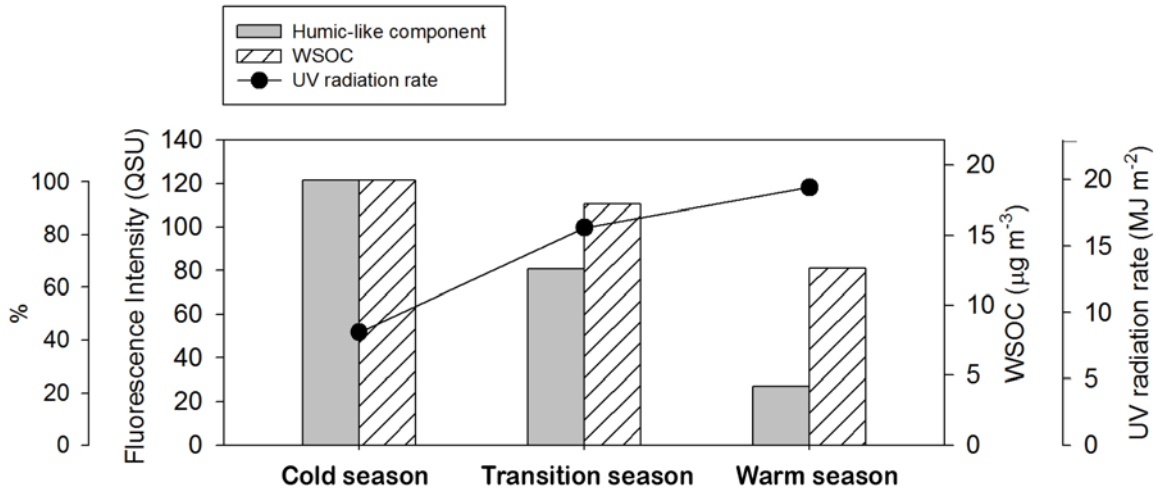

Figure 22. Seasonal variations of the fluorescence intensity of humic-like component, WSOC concentration, and UV radiation rate from cold (Oct–Dec), transition (Mar–May and late Sep–Oct), to warm seasons (Jun–Sep) in Seoul.

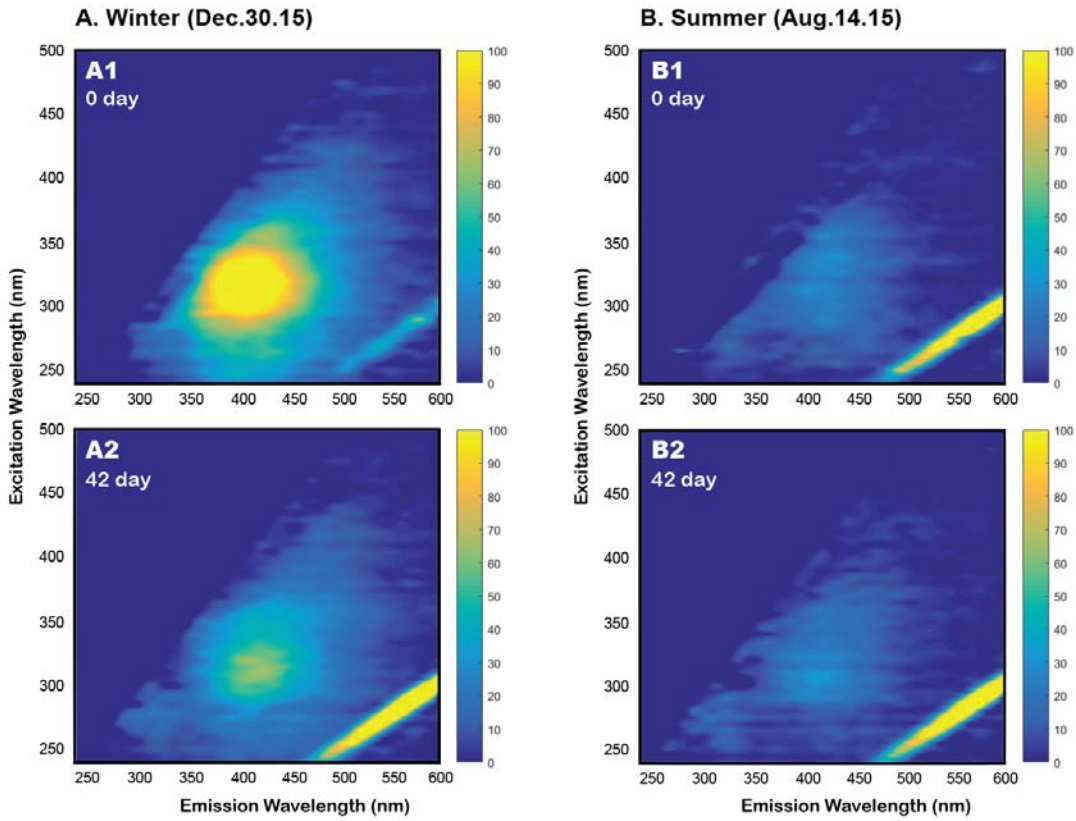

Figure 23. Contour plots of fluorescence EEM spectra for (A1) the non-irradiated initial and (A2) UV irradiated final aerosol WSOM samples collected during winter (Dec/30/15), and (B1) the non-irradiated initial and (B2) UV irradiated final aerosol WSOM samples collected during summer (Aug/14/15).

5. Conclusion

This study observed the characteristics of WSOM of ambient urban aerosols in Seoul, Korea. The WSOC concentration exhibited a regular variation over different seasons, while the carbon isotope abundance showed a significantly larger variation due to source variability. The WSOC is mainly derived from a terrestrial source emission. However, the contribution of the source intervention would be considerable depending on its source regions and regional climate system over different seasons.

Although the source of WSOC was greatly influenced by different factors, the fluorescence property and WSOC concentration of organic aerosols exhibited a similar seasonal variation. During warm season (Jun–early Sep), light absorbing organic aerosol, referred as HULIS fraction, was predominantly degraded by solar UV radiation. The results suggest that photo-induced degradation plays a significant role in optical property in both absorbance and fluorescence of WSOM and might be an important sink for the light absorbing organic aerosols in urban environment.

This study is very first approach providing a yearlong variation of fluorescence spectral properties and suggesting the photochemical degradation as an important sink mechanism of organic aerosols. The results from my research could have significant implications for a better understanding of the optical property of light absorbing organic aerosols and an estimating radiative budget of the global climate system in urban atmosphere. Furthermore, deposition fluxes of organic aerosols with different optical characteristics can have a significant role as a potential source of organic carbon to surface waters and, consequently, having major implications on global carbon cycle.

References

Andreae, M. and Gelencser, A. 2006. Black carbon or brown carbon? The nature of light-absorbing carbonaceous aerosols. Atmospheric Chemistry and Physics, 6, 3131–3148.

Birdwell, J. E. and Engel, A. S. 2010. Characterization of dissolved organic matter in cave and spring waters using UV-Vis absorbance and fluorescence spectroscopy. Organic Geochemistry, 41(3), 270–280.

Bosch, C., Andersson, A., Kirillova, E. N., Budhavant, K., Tiwari, S., Praveen, P. S., Russell, L. M., Beres, N. D., Ramanathan, V., and Gustafsson, O. 2014. Source-diagnostic dual-isotope composition and optical properties of water-soluble organic carbon and elemental carbon in the South Asian outflow intercepted over the Indian Ocean. Journal of Geophysical Research: Atmosphere, 119, 11743–11759.

Bro, R. 1997. PARAFAC. Tutorial and applications. Chemometrics and Intelligent Laboratory Systems, 38, 149–171.

Cachier, H. 1989. Isotopic characterization of carbonaceous aerosols. Aerosol Science and Technology, 10(2), 379–385.

Cao, J. J., Lee, S. C., Zhang, X. Y., Chow, J. C., An, Z. S., Ho, K. F., Watson, J. G., Fung, K., Wang, Y. Q., and Shen, Z. X. 2005. Characterization of airborne carbonate over a site near Asian dust source regions during spring 2002 and its climatic and environmental significance. Journal of Geophysical Research: Atmosphere, 110, D03203.

Cao, F., Zhang, S. C., Kawamura, K., and Zhang, Y. L. 2016. Inorganic markers, carbonaceous components and stable carbon isotope from biomass burning

aerosols in Northeast China. Science of the Total Environment, 572, 1244–1251.

Chen, Q., Ikemori, F., and Mochida, M. 2016. Light absorption and excitation-emission fluorescence of urban organic aerosol components and their relationship to chemical structure. Environmental Science and Technology, 50, 10859–10868.

Coble, P. G. 2007. Marine optical biogeochemistry: the chemistry of ocean color. Chemical Reviews, 107, 402–418.

Dentener, F., Drevet, J., Lamarque, J. F., Bey, I., Eickhout, B., Fiore, A. M., Hauglustaine, D., Horowitz, L. W., Krol, M., Kulshrestha, U. C., Lawrence, M., Galy-Lacaux, C., Rast, S., Shindell, D., Stevenson, D., Van Noije, T., Atherton, C., Bell, N., Bergman, D., Butler, T., Cofala, J., Collins, B., Doherty, R., Ellingsen. K., Galloway, J., Gauss, M., Montanaro, V., Muller, J. F., Pitari, G., Rodriguez, J., Sanderson, M., Solmon, F., Strahan, S., Schultz, M., Sudo, K., Szopa, S., and Wild, O. 2006. Nitrogen and sulfur deposition on regional and global scales: A multimodel evaluation. Global Biogeochemical Cycles, 20, GB4003.

Duarte, R. M. B. O. and Duarte, A. C. 2013. Atmospheric organic matter. Encyclopedia of Magnetic Resonance, 2(3), 415–426.

Fu, P., Kawamura, K., Chen, J., Qin, M., Ren, L., Sun, Y., Wang, Z., Barrie, L. A., Tachibana, E., Ding, A., and Yamashita, Y. 2015. Fluorescent water-soluble organic aerosols in the High Arctic atmosphere. Scientific Reports, 5, 9845.

Gabriel, R., Mayol-Bracero, O. L., and Andreae, M. O. 2002. Chemical characterization of submicron aerosol particles collected over the Indian Ocean. Journal of Geophysical Research: Atmosphere, 107, 8005.

Ghan, S. J. and Schwartz, S. E. 2007. Aerosol properties and processes: A path from field and laboratory measurements to global climate models. American Meteorological Society, 88(7), 1059–1083.

Gelencser, A., May, B., Simpson, D., Sanchez-Ochoa, A., Kasper-Giebl, A., Puxbaum, H., Caseiro, A., Pio, C., and Legrand, M. 2007. Source appointment of PM2.5 organic aerosol over Europe: Primary/secondary, natural/anthropogenic, and fossil/biogenic origin. Journal of Geophysical Research: Atmosphere, 112, D23S04.

Graber, E. R. and Rudich, Y. 2006. Atmospheric HULIS: How humic-like are they? A comprehensive and critical review. Atmospheric Chemistry and Physics, 6, 729–735.

Green, S. A. and Blough, N. V. 1994. Optical absorption and fluorescence properties of chromophoric dissolved organic matter in natural waters. Limnology and Oceanography, 39(8), 1903–1916.

Greenpeace. Silent killer: fine particulate matter. 2015. NGO. http://www.greenpeace.org/korea/Global/korea/publications/reports/climate-energy/2015/silentkillers_en.pdf.

Hecobian, A., Zhang, X., Zheng, M., Frank, N., Edgerton, E. S., and Weber, R. J. 2010. Water-soluble organic aerosol material and the light-absorption characteristics of aqueous extracts measured over the Southeastern United States. Atmospheric Chemistry and Physics, 10, 5965–5977.

Helms, J. R., Stubbins, A., Perdue, E. M., Green, N. W., Chen, H., and Mopper, K. 2013. Photochemical bleaching of oceanic dissolved organic matter and its effect on absorption spectral slope and fluorescence. Marine Chemistry, 155, 81–91.

Hoffer, A., Gelencser, A., Guyon, P., Kiss, G., Schmid, O., Frank, G. P., Artzxo, P., and Andreae, M. O. 2006. Optical properties of humic-like substances (HULIS) in biomass-burning aerosols. Atmospheric Chemistry and Physics, 6, 3563–3570.

Hu, X. and Zimmer, Y. 2013. China's Corn Production – Where to establish agri benchmark Farms in Corn. Agri Benchmark.

Huang, K., Fu, J. S., Hsu, N. C., Gao, Y., Dong, X., Tsay, S. C., and Lam, Y. F. 2012. Impact assessment of biomass burning on air quality in Southeast and East Asia during BASE-ASIA. Atmospheric Environment, 78, 291–302.

Huguet, A., Vacher, L., Relexans, S., Saubusse, S., Froidefond, J. M., and Parlanti, E. 2009. Properties of fluorescent dissolved organic matter in the Gironde Estuary. Organic Geochemistry, 40(6), 706–719.

Kanakidou, M., Seinfeld, J. H., Pandis, S. N., Barnes, I., Dentener, F. J., Facchini, M. C., Van Dingenen, R., Ervens, B., Nenes, A., Nielsen, C. J., Swietlicki, E., Putaud, J. P., Balkanski, Y., Fuzzi, S., Horth, J., Moortgat, G. K., Winterhalter, R., Myhre, C. E. L., Tsigaridis, K., Vignati, E., Stephanou, E. G., and Wilson, J. 2005. Organic aerosol and global climate modeling: a review. Atmospheric Chemistry and Physics, 5, 1053–1123.

Kelly, S. D., Stein, C., and Jickelle, T. D. 2005. Carbon and nitrogen isotopic analysis of atmospheric organic matter. Atmospheric Environment, 39(32), 6007–6011.

Kieber, R. J., Whitehead, R. F., Reid, S. N., Willey, J. D., and Seaton, P. J. 2006. Chromophoric dissolved organic matter (CDOM) in rainwater, Southeastern North Carolina, USA. Journal of Atmospheric Chemistry, 54(1), 21–41.

Kirillova, E. N., Andersson, A., Han, J., Lee, M., and Gustafsson, O. 2014a. Sources and light absorption of water-soluble organic carbon aerosols in the outflow from northern China. Atmospheric Chemistry and Physics, 14, 1413–1422.

Kirillova, E. N., Andersson, A., Tiwari, S., Srivastava, A. K., Bisht, D. S., and Gustafsson, O. 2014b. Water-soluble organic carbon aerosols during a full New Delhi winter: Isotope-based source appointment and optical properties. Journal of Geophysical Research: Atmosphere, 119, 3476–3485.

Kowalczuk, P., Durako, M. J., Young, H., Kahn, A. E., Copper, W. J., and Gonsior, M. 2009. Characterization of dissolved organic matter fluorescence in the South Atlantic Bight with use of PARAFAC model: Interannual variability. Marine Chemistry, 113(3–4), 182–196.

Lin, C. Y., Sheng, Y. F., Chen, W. N., Wang, Z., Kuo, C. H., Chen, W. C., and Yang, T. 2012. The impact of channel effect on Asian dust transport dynamics: a case in southeastern Asia. Atmospheric Chemistry and Physics, 12, 271–285.

Meng, Z., Zhang, R., Lin, W., Jia, X., Yu, X., Yu, X., and Wang, Gehui. 2014. Seasonal variation of ammonia and ammonium aerosol at a background

station in the Yangtze River delta region, China. Aerosol and Air Quality Research, 14, 756–766.

Mladenov, N., Lopez-Ramos, J., McKnight, D. M., and Reche, I. 2009. Alpine lake optical properties as sentinels of dust deposition and global change. Limnology and Oceanography, 54(6–2), 2386–2400.

Mladenov, N., Reche, I., Olmo, F. J., Lyamani, H., and Alados-Arboledas, L. 2010. Relationships between spectroscopic properties of high-altitude organic aerosols and sun photometry from ground-based remote sensing. Journal of Geophysical Research, 115, G00F11.

Murphy, K. R., Ruiz, G. M., Dunsmuir, W. T. M., and Waite, T. D. 2006. Optimized parameters for fluorescence-based verification of ballast water exchange by ships. Environmental Science and Technology, 40(7), 2357–2362.

Peltzer, E. T., Fry, B., Doering, P. H., McKenna, J. H., Norrman, B., and Zweifel, U. L. 1996. A comparison of methods for the measurement of dissolved organic carbon in natural waters. Marine Chemistry, 54(1-2), 85–96.

Poschl, U. 2005. Atmospheric aerosols: composition, transformation, climate and health effects. Angewandte Chemie International Edition, 44, 7520–7540.

Santos, P. S. M., Duarte, R. M. B. O., and Duarte, A. C. 2009. Absorption and fluorescence properties of rainwater during the cold season at a town in Western Portugal. Journal of Atmospheric Chemistry, 62(1), 45–57.

Singh, R., Kulshrestha, M. J., Kumar, B., and Chandra, S. 2016. Impact of anthropogenic emissions and open biomass burning on carbonaceous aerosols in urban and rural environment of Indo-Gangetic Plain. Air Quality, Atmosphere & Health, 9(7), 809–822.

Song, C., Zaveri, R. A., Alexander, M. L., Thorton, J. A., Madronich, S., Ortega, J. V., Zelenyuk, A., Yu, X. Y., Laskin, A., and Maughan, D. 2007. Effect of hydrophobic primary organic aerosol on secondary organic aerosol formation from ozonolysis of α–pinene. Geophysical Research Letters, 34, L20803.

Stedmon, C. A. and Bro, R. 2008. Characterizing dissolved organic matter fluorescence with parallel factor analysis: a tutorial. Limnology and Oceanography: Methods, 6(11), 572–579.

Stedmon, C. A. and Markager, S. 2005. Resolving the variability in dissolved organic matter fluorescence in a temperate estuary and its catchment using PARAFAC analysis. Limnology and Oceanography, 50(2), 686–697.

Stedmon, C. A., Markager, S., and Bro, R. 2003. Tracing dissolved organic matter in aquatic environment using a new approach to fluorescence spectroscopy. Marine Chemistry, 82(3–4), 239–254.

Stein, A. F., Draxler, R. R., Rolph, G. D., Stunder, B. J., Cohen, M. D., and Ngan, F. 2015. NOAA's HYSPLIT atmospheric transport and dispersion modeling system. American Meteorological Society, 96, 2059–2077.

Velapoldi, R. A. and Mielenz, K. D. 1980. Standard Reference Materials: A fluorescence standard reference material: Quinine Sulfate Dihydrate.

Wang, Y. Q., Zhang, X. Y., Arimoto, R., Cao, J. J., and Shen, Z. X. 2005. Characteristics of carbonate content and carbon and oxygen isotopic composition of northern China soil and dust aerosol and its application to tracing dust sources. Atmospheric Environment, 39(14), 2631–2642.

Wozniak, A. S., Bauer, J. E., and Dickhut, R. M. 2012. Characteristics of water-soluble organic carbon associated with aerosol particles in the eastern United States. Atmospheric Environment, 46, 181–188.

Yamashita, Y., Cory, R. M., Nishioka, J., Kuma, K., Tanoue, E., and Jaffe, R. 2010. Fluorescence characteristics of dissolved organic matter in the deep waters of the Okhotck Sea and the northwestern North Pacific Ocean. Deep-Sea Research Part II: Topical Studies in Oceanography, 57(16), 1478–1485.

Yamashita, Y., Jaffe, R., Maie, N., and Tanoue, E. 2008. Assessing the dynamics of dissolved organic matter (DOM) in coastal environment by excitation emission matrix fluorescence and parallel factor analysis (EEM-PARAFAC). Limnology and Oceanography, 53(5), 1900–1908.

Yan, G. and Kim, G. 2015. Sources and fluxes of organic nitrogen in precipitation over the southern East Sea/Sea of Japan. Atmospheric Chemistry and Physics, 15, 2761–2774.

Zappoli, S., Andracchio, A., Fuzzi, S., Facchini, M. C., Gelencser, A., Kiss, G., Krivacsy, Z., Molnar, A., Meszaros, E., Hansson, H. C., Rosman, K., and Zebuhr, Y. 1999. Inorganic, organic and macromolecular components of fine aerosol in different areas of Europe in relation to their water solubility. Atmospheric Environment, 33, 2733–2743.

Zepp, R. G., Sheldon, W. M., and Moran, M. A. 2004. Dissolved organic fluorophores in southeastern US coastal waters: Correction method for eliminating Rayleigh and Raman scattering peaks in excitation-emission matrices. Marine Chemistry, 89(1–4), 15–36.

Zhang, Y., Liu, X., Osburn, C. L., Wang, M., Qin, B., and Zhou, Y. 2013. Photobleaching response of different sources of chromophoric dissolved

organic matter exposed to natural solar radiation using absorption and excitation-emission matrix spectra. PLoS ONE, 8(10), e77515.

Zhou, S., Wang, Z., Gao, R., Xue, L., Yuan, C., Wang, T., Gao, X., Wang, X., Nie, W., Xu, Z., Zhang, Q., and Wang, W. 2012. Formation of secondary organic carbon and long-range transport of carbonaceous aerosols at Mount Heng in South China. Atmospheric Environment, 63, 203–212.

Appendix

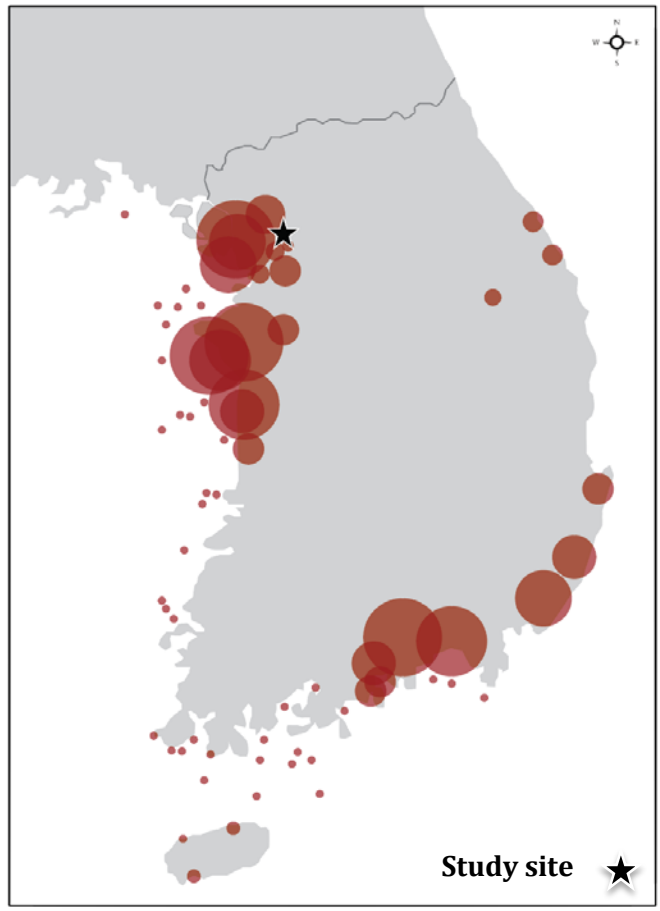

Figure A. Distributions of coal power plants in South Korea.

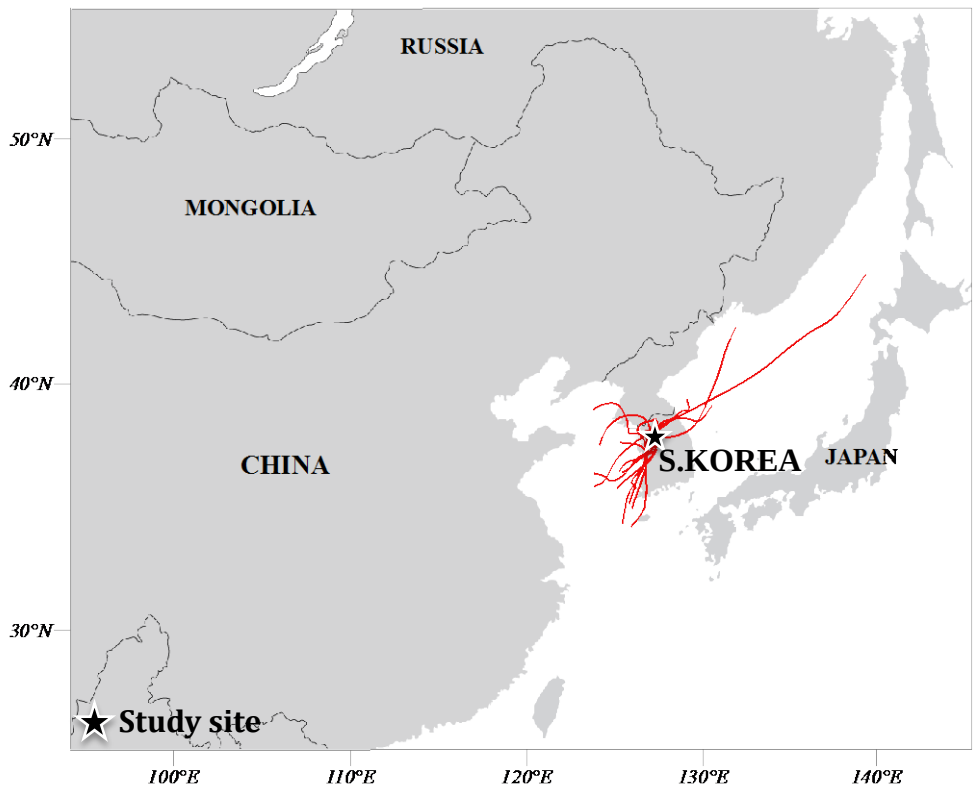

Figure B. Map of geographical region around study site along with 10-day air mass back trajectories with NOAA HYSPLIT model during August 2015.

국문초록

대기 중 용존유기에어로졸은 태양복사에너지의 균형, 구름의 생성, 대기 중 이동 및 침적 등 전 지구적 기후시스템과 관련한 대기 형성 과정에 매우 중요하다. 특히 용존유기에어로졸 중 자외선과 가시광선 범위의 에너지를 흡수하는 성질의 유기탄소종인 갈색탄소 (Brown carbon)와 휴믹한 성질의 물질 HULIS (humic-like substances)는 대기 기후에 상당히 중요한 역할을 한다.

용존유기탄소의 양은 전체 유기에어로졸 중 약 10-80% 를 차지하며, 그 중 약 15-60% 는 HULIS 로 이루어져 있는데 이들은 미생물 분해 등으로 형성되는 육지나 해양 기원의 유색용존유기물의 휴믹 물질과 매우 유사한 특성과 성질을 보인다. 이처럼 대기 중의 용존유기에어로졸이 전 지구적 생지화학 순환에 크게 영향력이 있음에도 불구하고, 그에 대한 기원부터 형성과 제거 그리고 화학적 구성, 광학적 특성에 대해서는 잘 알려져 있지 않다. 따라서 본 연구에서는 대기 중 용존유기에어로졸의 기원과 제거 기작 및 광학적 특성의 이해를 위해 서울 도심에서 2015 년 3 월부터 1 년간 대기 에어로졸의 용존유기탄소와 용존유기질소의 농도, 무기 이온 농도, 탄소 안정동위원소비, 유색용존유기물의 형광 세기 (intensity)를 측정하였다.

대기 에어로졸 중 용존유기탄소의 농도는 3.1 에서 39.5 $\mu g\ m^{-3}$ (평균: 16.1 $\mu g\ m^{-3}$)의 범위와 함께 계절적 변화를 보였고, 최고 농도는 봄과 겨울 동안 (3-5 월, 10-1 월) 최저 농도는 여름에 (6-9 월)

관측되었다. 반면 용존유기질소는 0.8 에서 81.7 $\mu g\ m^{-3}$ (평균: 14.5 $\mu g\ m^{-3}$)으로 계절에 따라 광범위한 농도 차를 보였다. 에어로졸 중 용존유기탄소의 안정동위원소비값은 -21.0 에서 -27.5‰ 의 범위를 보였으며, 연간 평균은 -24.0‰ 로 나타났다. 이 값은 육상 기원 물질과 인간활동에 의해 배출된 물질의 탄소 안정동위원소비값의 범위와도 거의 일치한다. 무기이온 분석 결과 서울 도심 내의 용존유기탄소가 주로 육상 기원 물질의 연소로부터 기원한 것으로 나타났다. 공기 역 궤적 수치모델 (air mass back trajectory model) 결과 여름을 제외한 모든 계절 동안 우리나라에 영향을 미치는 기류는 중앙아시아 및 중국의 사막지역 등 대륙 내부로부터 기원되는 것으로 나타났다. 또한 한반도 지역은 아시아 대륙의 풍하 측에 위치해 있어 대륙기원의 다양한 물질의 유입이 본 연구지역의 용존유기에어로졸 특성에 상당한 영향을 미치는 것으로 보인다.

대기 에어로졸 중 유색용존유기물 형광세기의 계절적 변화는 용존유기탄소의 계절적 변화와 매우 유사하게 나타났다. 유색용존유기에어로졸의 특성을 분석한 결과, 여름철 자외선 방사 량이 약 2 배 이상 증가함에 따라 HULIS 의 형광세기는 약 80% 감소했고, 에어로졸 중 용존유기탄소 농도의 경우 약 30% 가량 감소했다. 또한 HULIS 의 형광세기와 자외선 방사 량은 음의 상관관계 (r^2=0.4)를 나타냈다. 따라서, 대기 에어로졸 중 HULIS 가 우선적으로 광화학적 분해에 의해 감소하는 추세를 보여준다. 이는 대기 중 광분해가 용존유기에어로졸의 중요한 제거 기작임을 보여준다. 이러한 결과는 실험실 실험 결과와도 유사하게 나타났다.

본 연구결과에 따르면 서울 도심 대기 중 용존유기에어로졸이 주로 육상 기원 물질의 연소로부터 기원하며, 계절에 따라 연구지역의 지리와 기후적 특성에 영향을 받는 것으로 나타났다. 에어로졸 중 유색용존유기물은 대기 복사에너지에 의한 광화학적 반응에 우선적으로 영향을 받는데, 이는 복사에너지에 의한 광화학적 분해가 대기 광학적 특성을 이해하는데 매우 중요한 역할을 하며, 용존유기에어로졸 중 에너지를 흡수하는 성질의 유기탄소의 중요한 제거 기작으로 보인다.

주요어: 유기 에어로졸, 용존유기물, 용존유기탄소, HULIS, 유색용존유기물, 광분해

학번: 2014-21312